Research Square

Preprints are preliminary reports that have not undergone peer review.
They should not be considered conclusive, used to inform clinical practice,
or referenced by the media as validated information.

PDGF Signaling Modulates Autophagy Following Cellular Stress in Cranial Neural Crest Cells Across Vertebrate Species

Johann Eberhart

eberhart@austin.utexas.edu

University of Texas at Austin https://orcid.org/0000-0001-5258-2477

Shuge Sun

University of Texas at Austin

Lilly Walsh

University of Texas at Austin

Ritika Ghosal

University of Texas at Austin

Scott Tucker

University of Texas at Austin

Janeta Zoldan

University of Texas at Austin

Article

Keywords: Pdgf signaling, autophagy, raptor, mTOR, neural crest cell, craniofacial development, phosphoproteomics, Fetal alcohol syndrome

Posted Date: September 28th, 2026

DOI: https://doi.org/10.21203/rs.3.rs-10923857/v1

License: This work is licensed under a Creative Commons Attribution 4.0 International License.
Read Full License

Additional Declarations: There is **NO** Competing Interest.

PDGF Signaling Modulates Autophagy Following Cellular Stress in Cranial Neural Crest Cells Across Vertebrate Species

Shuge Sun[1], Lilly Walsh[1], Ritika Ghosal[1], Scott K. Tucker[2], Janet Zoldan[3], Johann K. Eberhart[1].

[1]Department of Molecular Biosciences, Waggoner Center for Alcohol and Addiction Research and Institute for Neuroscience, The University of Texas, Austin, TX 78712, USA.

[2]Current address: Center for Craniofacial Innovation, Children's Hospital of Philadelphia, Philadelphia, PA 19104, USA

[3]Department of Biomedical Engineering, The University of Texas, Austin, TX 78712, USA.

shugesun@utexas.edu

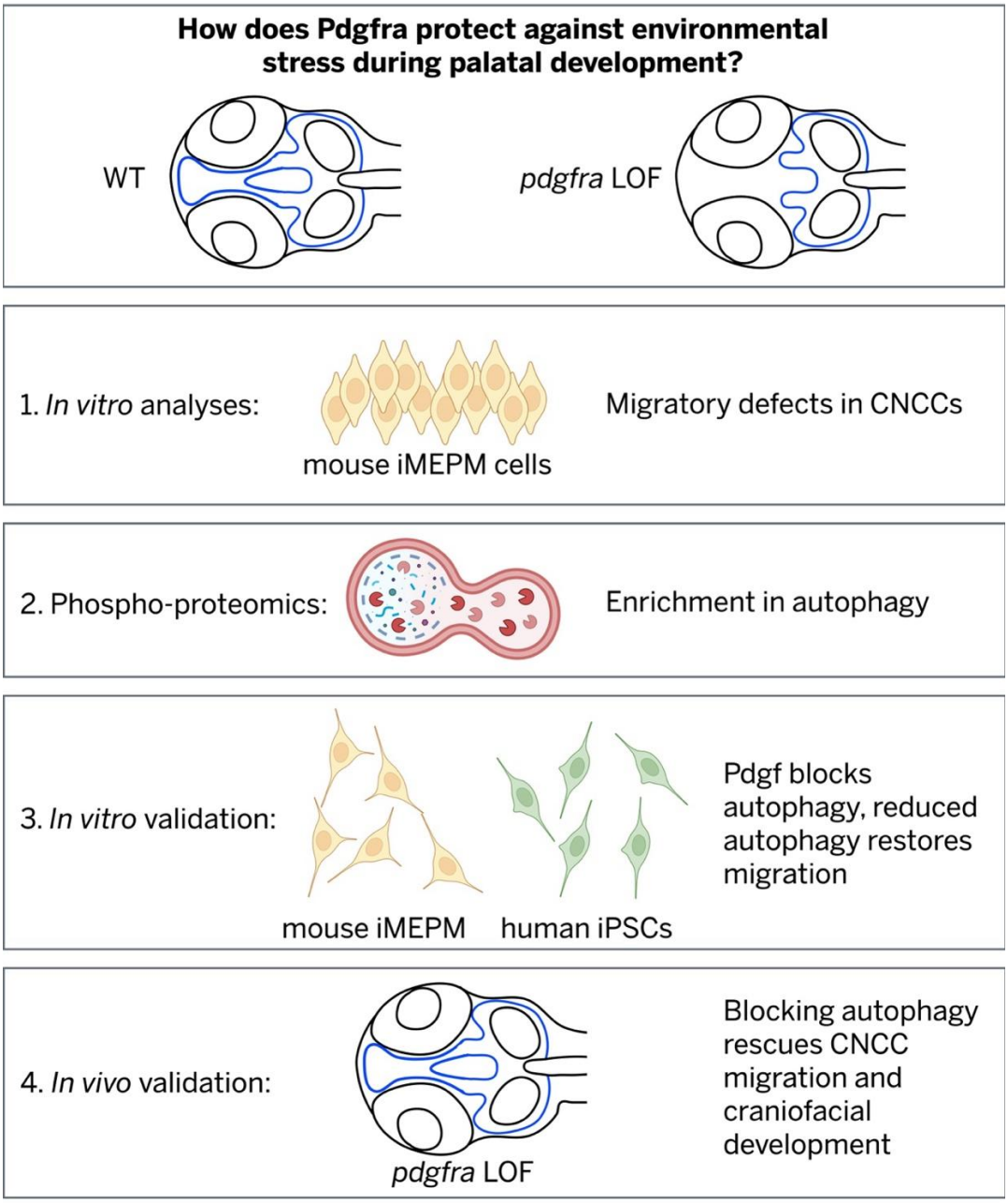
eberhart@austin.utexas.edu

Summary

Platelet-derived growth factor receptor-a (Pdgfra) signaling is essential for development of numerous organ systems including the craniofacial skeleton. Cranial neural crest cells generate most of the craniofacial skeleton and require Pdgfra signaling. Reductions in Pdgfra signaling also sensitizes embryos to craniofacial defects due to environmental perturbation. Here, we investigate how ethanol exposure intersects with Pdgfra signaling to alter neural crest cell behavior and craniofacial development combining *in vitro* and *in vivo* approaches. Using a mouse neural crest-derived cell line (iMEPM), we identify the concentration of ethanol that disrupts Pdgfra-mediated cellular behaviors. We perform phosphoproteomic analyses and find that ethanol exposure alters several pathways, including autophagy. We find that Pdgfra signaling protects iMEPM cells from ethanol-induced autophagy and inhibiting autophagy restores migration in exposed cells. We demonstrate that this function of Pdgf signaling is conserved in humans, using neural crest-like cells differentiated from iPSCs. We validate the *in vivo* relevance of Pdgfra signaling in modulating the response to environmental perturbation in a zebrafish model. We find that genetic elevation of autophagy, via *raptor* mutation, sensitizes *pdgfra* mutants and heterozygotes to

craniofacial defects. We also show that inhibiting autophagy partially rescues ethanol-induced craniofacial defects and neural crest cell migration in *pdgfra*-mutant and heterozygous zebrafish. Our findings reveal a novel role of Pdgf signaling in modulating autophagy, thereby influencing susceptibility to environmental stress.

Graphical Abstract:



Keywords: Pdgf signaling, autophagy, raptor, mTOR, neural crest cell, craniofacial development, phosphoproteomics, Fetal alcohol syndrome

Introduction

Cranial neural crest cells (CNCCs) are a transient, multipotent population that gives rise to most of the vertebrate facial skeleton, cartilage, smooth muscle, and connective tissues. Craniofacial development depends on the precise coordination of migration, proliferation, survival, and differentiation of CNCCs.[1-4] Originating at the neural plate border, CNCCs undergo an epithelial-to-mesenchymal transition and migrate to form a wide variety of cell types.[5] Their behaviors are guided by tightly regulated signaling interactions, and even subtle perturbations in CNCC migration cause congenital anomalies such as cleft lip/palate, frontonasal dysplasia, and micrognathia.[6,7] CNCCs are sensitive to both genetic and environmental perturbations and understanding the mechanisms of gene-environment interactions will provide great insight into craniofacial birth defects.

Among the pathways essential for CNCC morphogenesis, platelet-derived growth factor receptor α (Pdgfra) signaling is a key regulator of craniofacial patterning across vertebrate species.[8-10] In both mouse and zebrafish, *Pdgfra* mutants exhibit severe midfacial clefting, palatal defects, and CNCC migration abnormalities.[9-13] Consistent with a conserved role in craniofacial development, variants in PDGFRA and one of its ligands, PDGFC, have been associated with nonsyndromic orofacial clefting in humans.[14-16] In zebrafish, it has been shown that PDGF-AA likely functions as a short-range chemoattractant guiding rostrally migrating CNCCs around the optic stalk toward the oral ectoderm in zebrafish.[10]

Ethanol is one of the most common environmental teratogens and the leading preventable cause of birth defects. It disrupts multiple aspects of CNCC biology, including migration, oxidative stress and ROS accumulation, apoptosis, and key morphogen pathways such as SHH, BMP, and WNT.[17] Craniofacial abnormalities such as midfacial hypoplasia, short palpebral fissures, smooth philtra, and palatal defects are common features of FASD and reflect ethanol's profound impact on CNCC.[17-19] Mechanistic understanding of these defects has been advanced through zebrafish models of ethanol teratogenesis, which reveal dose-dependent disruptions in CNCC migration, brain patterning, and midline morphogenesis.[20]

Genetic studies in zebrafish identified *pdgfra* as a locus conferring heightened sensitivity to ethanol exposure.[10] Ethanol-treated *pdgfra* heterozygotes and mutants exhibit craniofacial defects that are more severe than those observed in unexposed heterozygotes and mutants. These findings suggest that partial loss of Pdgfra function predisposes embryos to ethanol-induced craniofacial disruption and that ethanol uniquely perturbs Pdgf-dependent developmental processes. However, whether ethanol interferes with PDGF ligand binding, receptor trafficking, kinase activation, or downstream intracellular effectors has remained unclear. Given the complexity and rapid dynamics of Pdgf-dependent signaling, a systems-level approach is required to define how ethanol alters these signaling networks.

Phosphoproteomic profiling enables unbiased, systems-level analysis of dynamic phosphorylation events downstream of receptor activation. This allows for a comprehensive assessment of how ethanol disrupts signaling networks and how Pdgf signaling may protect against these disruptions. Developmental and *in silico* studies have used phosphoproteomics to uncover regulators of cell cycle, cytoskeletal remodeling, revealing mechanistic insights into biological function in healthy and disease contexts.[21,22]. Applying this approach to ethanol-exposed CNCC-like cells enables identification of the signaling modules most sensitive to teratogenic stress and clarifies how PDGF-AA may restore disrupted pathways.

In this study, we integrate phosphoproteomic profiling in mouse-derived cells with analyses in human neural crest-like cells and an *in vivo* zebrafish system to dissect how ethanol perturbs cellular signaling pathways during craniofacial development. We find that ethanol disrupts PDGF-AA-mediated migration and proliferation but does not compromise Pdgfra activation. Phosphoproteomics identified autophagy and Rho-GTPase activity as processes disrupted by ethanol. In vitro analyses in mouse and human cells demonstrated a strong effect of Pdgf signaling in mitigating autophagy and restoring migration. We validate the effect of autophagy on migration in *pdgfra* heterozygous and mutation zebrafish. Together, these approaches provide a comprehensive framework for understanding how Pdgf signaling supports neural crest resilience under teratogenic stress and identify mechanistic targets with potential relevance for preventing craniofacial abnormalities associated with FASD.

Results

Ethanol attenuates PDGF-AA-mediated cranial neural crest cell (CNCC) behaviors

To investigate how ethanol modulates Pdgf-dependent cell behaviors, we used a mouse neural crest-derived cell line (iMEPM) previously demonstrated to respond robustly to PDGF stimulation.[23] An evolutionary conserved function of Pdgfra signaling is neural crest cell migration. [8,10,12] To examine how ethanol affects Pdgf-mediated migration of CNCCs, we first conducted a dose-response to determine the lowest concentration of ethanol that disrupts migration (Figure 1A). We initially stimulated iMEPM cells with 30 ng/mL recombinant PDGF-AA because concentrations in the 10~50 ng/mL range are widely reported to produce robust and near-maximal activation of Pdgfra signaling.[24] Stimulated cells were cultured in increasing concentrations of ethanol from 0% to 1.5%. Migration was quantified by measuring the change in scratch width before and after treatment. Migration was unaffected at 0.5% and 0.75% ethanol but was significantly reduced at 1.0% and 1.5% ($p < 0.0001$), with no further inhibition observed above 1.0% (Figure 1A). Therefore, 1% ethanol was used for subsequent experiments.

To determine the effects of ethanol on PDGF-stimulated CNCC migration, we treated iMEPM cells with low (10 ng/mL) and high (30 ng/mL) doses of PDGF-AA in the absence or presence of 1% ethanol (see Figure 1B for example before and after images). In the absence of ethanol, PDGF-AA significantly stimulated migration at both low and high concentrations, revealing the strong influence of PDGF-AA on CNCC migration (Figure 1C). However, in the presence of 1% ethanol, migration decreased compared to PDGF-AA treatment alone especially at high ligand concentrations, which suggests that ethanol inhibits the pro-migratory effects of PDGF-AA (Figure 1C). To control for an involvement of proliferation in our results, we repeated the assay while blocking proliferation with 1 μM of palbociclib (Figure 1C). When combined with 30 ng/mL PDGF-AA, cells migrated a comparable distance to those treated with PDGF-AA alone, indicating that wound closure was not due to proliferation.

Pdgfra has also been demonstrated to be involved in proliferation.[25] We used BrdU incorporation to assess the effects of ethanol on CNCC proliferation in the

presence or absence of PDGF-AA stimulation. Serum-starved cells were incubated with 1% ethanol, PDGF-AA (10 or 30 ng/mL), or a combination of both for 24 hours, followed by a 1-hour BrdU incubation (Figure S1). In the ethanol-treated group, fewer than 30% of cells incorporated BrdU, indicating reduced proliferation relative to control (~45% of cells). By contrast, PDGF-AA increased proliferation in a dose-dependent manner to ~70% and ~95% at 10 and 30 ng/mL, respectively. The addition of ethanol significantly blunted this response. Specifically, only ~15% of cells incorporated BrdU in the 1% EtOH + 10 ng/mL PDGF-AA group, and ~50% in the 1% EtOH + 30 ng/mL PDGF-AA group. Cells treated with palbociclib displayed proliferation rates comparable to those exposed to 1% ethanol. This indicates that 1% ethanol suppresses proliferative activity to a basal level equivalent to pharmacological cell cycle inhibition. Notably, only the high dose PDGF-AA (30 ng/mL) was able to partially counteract ethanol-induced proliferative suppression, restoring proliferation to a level comparable to that seen with low-dose PDGF-AA alone. These findings suggest that ethanol disrupts cell cycle progression and attenuates the mitogenic response to PDGF-AA. Therefore, ethanol attenuates Pdgfra-dependent cell behaviors in vitro and we focus on migration here.

Pdgfra expression and phosphorylation are not altered by EtOH

Ethanol could exert these effects by reducing the levels or activation of Pdgfra. Immunoblot analyses for total Pdgfra protein revealed that levels were unchanged by any treatment (Figure S2). We next investigated whether ethanol modulates receptor activation in CNCCs. We used HCR™ immunofluorescence to quantify p-Pdgfra levels following acute ligand stimulation (Figure S3). Cells were grown to approximately 90% confluency, serum-starved overnight to synchronize the cell cycle, and then treated for 5 minutes with 1% ethanol, PDGF-AA (30 ng/mL), or a combination of both. Ethanol treatment did not significantly alter phosphorylated Pdgfra levels compared to the control group (Figure 2A, B, E). In contrast, stimulation with PDGF-AA, either alone or together with ethanol, robustly increased Pdgfra phosphorylation, confirming receptor activation (Figure 2C, D, E). These results indicate that ethanol does not affect Pdgfra protein abundance or ligand-induced signaling activation, suggesting that the impairment to Pdgf-dependent cell behaviors is not due to reduced receptor signaling at the membrane.

Ethanol alters the Phosphoproteome

To understand how ethanol alters signaling pathways mediating neural crest cell behaviors, we performed a global phosphoproteomic analysis.[26] We sought to identify pathways that were altered by ethanol exposure and were restored with Pdgfra signaling. Protein lysates were harvested from cells treated for 5 minutes with 1% ethanol, 30 ng/mL PDGF-AA, or a combination of both (n = 4/group). Approximately one hundred phosphoproteins were significantly changed with high confidence (at least two counts) (Log_2 (FC) > 1, $p < 0.05$) under each condition compared to control (Figure 2). We used immunoblot analyses to validate the phosphorylation changes caused by ethanol exposure. We used phospho-specific antibodies to Grk2 and Dnmt1 and found that the levels of phosphorylate protein was significantly reduced in ethanol treated cells (Figure S4A). We used phos-tag immunoblotting to detect levels of Pak3. With this technique, the phosphorylated form of the protein runs at a higher molecular weight. We see substantial reduction in the levels of phospho-Pak3 (Figure S4B). Interestingly, there is also a reduction in the levels of unphosphorylated Pak3, suggesting the differences in Pak3 activation are due to differences in protein abundance. We also compared our PDGF-AA-stimulated dataset with a previously published set of PDGF-responsive phospho-AKT targets in MEPM cells. Despite the shorter stimulation period in our study (5 min versus 15 min previously), approximately 80% of the detected phosphoproteins overlapped, further validating our approach (Table S1).

Hierarchical clustering of these proteins displayed in heatmap demonstrated treatment-specific patterns (Figure 2A). Compared to control, we identified 77, 60 and 53 downregulated phospho-peptides in the ethanol, PDGF-AA, and co-exposed groups, respectively. We found that 43 of the 77 peptides were uniquely downregulated in the ethanol group, relative to all other groups (Figure 2B, Tables S2-S5). Similar analyses with upregulated phospho-peptides identified 29, 49 and 47 proteins in the ethanol, PDGF-AA, and co-exposed groups (Figure 2B, Table S2-S5). Only 3 phospho-peptides were uniquely upregulated in the ethanol exposed group.

We used Gene Ontology (Figure S5) and String analysis (Figure 2D) to identify potential pathways disrupted by ethanol. GO terms related to small GTPase signaling were enriched in all 3 groups. Members of this family, including Rac1 and RhoA, are

well-characterized downstream effectors of Pdgf signaling that control cytoskeletal remodeling, directed migration, and cell survival.[27,28] Notably, macroautophagy and the SNARE complex were only enriched in the EtOH vs. Control comparison. We selected "Textmining", "Experiments", and "Databases" as our interaction sources for STRING analysis. STRING analysis on the EtOH vs Control group (Figure 3D)[29] identified the RSC-type complex (5 genes), Rho GTPases activate PAKs (5 genes), and SNARE interactions in vesicular transport (4 genes) as the most highly enriched modules. The identified SNARE complex members, Atg9a, Vamp8, Snap29 and Stx7 are all involved in autophagy.

The down regulation of mTOR and Tecpr2 phosphorylation (Figure 2A) further suggests the involvement of autophagy in the ethanol-treated group[30,31]. This observation is consistent with prior findings from our lab showing that pharmacologic inhibition of mTOR phenocopies the ethanol-induced craniofacial defects in *pdgfra* heterozygotes and mutants, and that *raptor* mutants exhibit elevated autophagy accompanied by neural crest cell death and craniofacial defects.[13,32] Together, these studies suggest that excessive autophagy is associated with craniofacial vulnerability in the context of impaired Pdgf signaling, raising the possibility that ethanol-induced autophagic dysregulation contributes to the observed defects.

Pdgf signaling rescues ethanol-induced autophagy *in vitro*

The RSC complex regulates chromatin accessibility, which could mis-regulate expression of genes involved in migration. Tag-sequencing of ethanol exposed cells, revealed only 13 differentially regulated genes following 1 hour of ethanol exposure (Table S6; Figure S6). Thus, at this time point, RSC complex mis-regulation is not causing widespread transcriptional changes. However, one of these genes was *Rhob*, which along with one of the other identified modules, Rho GTPases, could alter migration. However, activation of Rho-GTPases failed to restore migration *in vitro* (data not shown). In ethanol-exposed *pdgfra* heterozygotes, treatment with small GTPase activators partially restored craniofacial morphology (Figure S7; $n \geq 8$, $p < 0.0001$). However, the same treatment failed to rescue ethanol-induced craniofacial defects in *pdgfra* homozygous mutants (Figure S7; $n \geq 3$). While the RSC complex and Rho-

GTPase function may play a role in ethanol teratogenesis, we turned our analyses to autophagy.

To experimentally validate the autophagy signature, we examined autophagic activity using LysoTracker staining. We conducted an ethanol dose-response experiment (0.5 to 2%) and found that 1% was the lowest concentration of ethanol that significantly elevated LysoTracker levels in cells (Figure S8), consistent with our findings for ethanol's disruption of migration. Higher doses of ethanol further elevated autophagy demonstrating that 1% ethanol does not result in a maximal response in autophagy. We next treated cells with 30 ng/mL PDGF-AA, alone or in combination with 1% ethanol (Figure 3A-E). PDGF-AA alone did not alter LysoTracker signal relative to control cells, suggesting that PDGF-AA itself does not substantially alter basal autophagic activity in cell culture. Co-treatment with ethanol and PDGF-AA reduced signal to levels indistinguishable from the control and PDGF-AA groups, demonstrating that Pdgfra signaling modulates autophagy induced by ethanol (Figure 3E). Thus, Pdgfra signaling reduces autophagy and improves migration of neural crest-derived cells in culture.

To determine if autophagy results in migratory defects, we reduced the levels of autophagy in exposed cells via Chloroquine, a pharmacological inhibitor of autophagy. Concentrations of chloroquine commonly used in cell culture to reduce autophagy range from 25 to 200 μM. However, concentrations as low as 15 μM have been shown to inhibit mouse palatal mesenchyme cell migration[33]. To find a lower dose that effectively reduces autophagy and may be compatible with migratory assays, we compared the effects of 10 and 25 μM chloroquine on ethanol-induced autophagy (Figure S9). Relative to levels in the ethanol alone group, LysoTracker signal was significantly reduced in cells treated with 1% ethanol and 10 uM or 25 uM chloroquine (Figure S9), with 10 uM chloroquine restoring Lysotracker signal to baseline levels (Figure S9 A, C, E). These data further validate our phosphoproteomic findings and demonstrate that acute ethanol exposure at 1% reproducibly promotes autophagic activity in cranial neural crest-derived cells that can be blocked by chloroquine.

This finding led us to test the effects of 10 μM chloroquine on neural crest cell migration (Figure 4). We found that chloroquine had no effect on basal migration of

neural crest cells, with control, ethanol exposed and chloroquine exposed cells migrating similar distances. Interestingly, combined treatment of ethanol and chloroquine significant increased migration in the absence of PDGF stimulation ($n = 12$, $p < 0.0001$) to a level even higher than in stimulated cells exposed to ethanol. Combining PDGF-AA stimulation and chloroquine did not further enhance migration of cells exposed to ethanol, relative to PDGF-AA or chloroquine separately, suggesting the primary function of Pdgfra signaling in the context of ethanol-induced migratory defects is mediating autophagy.

The role of PDGFRA signaling is conserved in human neural crest-like cells

To determine whether this mechanism extends beyond mouse neural crest cells, we next tested human iPSC-derived migratory neural crest-like cells. We differentiated human iPSCs into migratory neural crest-like cells as previously described (Figure S10).[34] As in the mouse cell line, we find that exposure to 1% ethanol significantly elevates autophagy (Figure 5B, E). Levels of autophagy are restored to baseline with the co-administration of PDGF-AA (Figure 5D, E) but has no effect on the baseline levels of autophagy (Figure 5A, C, E). Thus, PDGF signaling plays a role in modulating autophagy following cell stress in human cells as well.

Unlike iMEPM cells, which exhibit a low basal level of migration, human induced neural crest-like cells exhibit a robust basal level of migration in the presence or absence of PDGF-AA (Figure 6A, C, E). This migration is dramatically diminished by ethanol exposure, and PDGF-AA stimulation improves wound closure (Figure 6B, D, E). These results demonstrate a conserved function of PDGFRA signaling in modulating autophagy and neural crest cell migration in humans.

***In vivo* genetic interaction between *pdgfra* and *raptor* during craniofacial morphogenesis**

To test the function of autophagy during neural crest cell migration *in vivo* we moved to zebrafish. Raptor (Regulatory-associated protein of mTOR) is an essential component of mTORC1 (mechanistic Target of Rapamycin Complex 1), the master negative regulator of autophagy. Loss of Raptor diminishes mTORC1 activity and leads to elevated autophagy[35]. We previously demonstrated that this elevated autophagy leads to craniofacial defects in zebrafish[32]. To test if genetically elevating autophagy

phenocopied the effects of ethanol on *pdgfra* mutants and heterozygotes, we analyzed the effect of allelic combinations of *raptor* and *pdgfra* on craniofacial development (Figure S11). As expected, *pdgfra* homozygous mutants exhibited characteristic anterior neurocranial defects, including clefting of the ethmoid plate and shortened trabeculae[13] (Figure S11G, J). In comparison, *raptor* mutants displayed relatively minor craniofacial abnormalities in fish wild-type or heterozygous for *pdgfra* (Figure S11C, F, J). We note though that there is a significant reduction in *pdgfra*$^{+/-}$;*raptor*$^{-/-}$ fish relative to wild-type fish (Figure S11F, J). Thus, in the presence of Pdgfra signaling, elevated autophagy does not have a profound effect on craniofacial development.

However, combined loss of *pdgfra* and *raptor* produced a markedly exacerbated phenotype. Double mutants had near complete loss of the anterior neurocranium (Figure S11I, J), similar to what is observed in ethanol-treated *pdgfra* mutants.[13] This phenotype was substantially more severe than either single mutant, demonstrating a strong genetic interaction between *pdgfra* and *raptor* (Figure S11J, $n \geq 8$ per group, $p < 0.0001$). These findings provide *in vivo* genetic support for a model in which Pdgfra function buffers against elevated autophagy during craniofacial development.

Inhibition of autophagy rescues craniofacial morphology and neural crest cell migration in exposed *pdgfra* heterozygotes and homozygotes

Previous studies from our lab[13] demonstrated that ethanol exposure induces palate defects in *pdgfra* heterozygotes and exacerbates craniofacial malformations in *pdgfra* mutants. If increased autophagy contributes to the craniofacial abnormalities observed in *pdgfra* mutants and heterozygotes, then pharmacological suppression of autophagy should protect against these defects. To test this prediction, we co-exposed offspring of *pdgfra* heterozygotes to ethanol and chloroquine from 6 h to 4 dpf (Figure 7). In both *pdgfra* heterozygous and homozygous mutants, ethanol treatment significantly reduces the length of the anterior neurocranium relative to unexposed fish of the same genotype (Figure 7E, H, J). Chloroquine co-exposure restored the neurocranium in *pdgfra* heterozygotes back to wild-type length and significantly improved the length in mutants (Figure 7F, I, J). In mutants, ethanol exposure results in a complete and invariant loss of the anterior neurocranium and the penetrance of this effect is lessened by co-exposure (Figure 7K). These findings support a model in which

Pdgf signaling buffers against ethanol-induced autophagic dysregulation, thereby protecting craniofacial development.

We previously demonstrated that Pdgfra signaling was necessary for the proper migration of neural crest cells that populate the palatal skeleton.[10] We analyzed the distribution of neural crest cells to determine if autophagy was involved in neural crest cell migration defects *in vivo*. The disruption in neural crest cell migration in *pdgfra* mutants can be observed by the failure of these cells to enter the region posterior and ventral to the eye en route to the maxillary domain (Figure 8).[10] Wild-type fish display few gross defects in neural crest cell migration regardless of treatment (Figure 8A, B, C, M, n=12, 7 and 8, respectively). Ethanol significantly elevates gross migratory defects in heterozygotes (Figure 8D, E; n=21 and 13) and chloroquine exposure results in a level of defects intermediate between the two (Figure 8F, M; n=17). In untreated *pdgfra* mutants, over 75% of embryos display a failure of migration (Figure 8G, J, M; n=12). This increases to 100% in ethanol-exposed mutants (Figure 8H, K, M; n=16) and is significantly reduced, to 68%, via co-exposure to chloroquine (Figure 8I, L, M; n=19). There is a range in severity of migratory defects in mutants, which appears most severe in ethanol-exposed mutants relative to untreated or chloroquine treated mutants (Figure 8H, K). Thus, the effect of autophagy on migration is conserved across *in vitro* and *in vivo* systems.

Discussion

Using phosphoproteomic profiling, we identified autophagy as a primary response to ethanol-induced cellular stress. We demonstrate that PDGFRA signaling reduces stress-induced autophagy in both mouse and human-derived neural crest cells. Reducing autophagy results in the re-establishment of PDGFRA-dependent neural crest cell migration. Using zebrafish, we go on to demonstrate that elevated autophagy results in *pdgfra*-dependent craniofacial and neural crest cell migration defects. This is the first demonstration that PDGFRA signaling buffers against autophagy. Our demonstration that this is conserved between human, mouse and zebrafish strongly suggests that this is an ancient function of the PDGF pathway.

Linking PDGF signaling to autophagy

While there is evidence linking autophagy and PDGFRA signaling in tumor growth, this is via autophagy of the receptor itself reducing PDGF signaling[36,37], not PDGF signaling modulating autophagy. We find no alteration in the total or phospho-protein levels of Pdgfra in ethanol exposed mouse cells, demonstrating that this function may be specific to cancer and not a general role of autophagy modulating Pdgf signaling.

A previous proteomic analysis of targets of Pdgfra signaling in mouse did not detect an autophagy signature.[25] Consistent with this publication, we find no enrichment for autophagy in PDGF-AA stimulated cells. This is perhaps not surprising as there is likely to be little basal cell stress or autophagy in cell culture. This is also true in animal model systems where the environment is tightly controlled. Thus, PDGFRA function has only being partially assayed.

The mTOR pathway receives numerous inputs and is the master regulator of autophagy. One such input is growth factor signaling, notably the Insulin Growth Factor pathway which activates mTORC1 through the PI3K-AKT pathway[38]. PI3K-AKT is the predominant pathway used by PDGFRA in craniofacial development[25]. In gastrointestinal stromal tumors activating mutations in PDGFRA associate with elevated mTORC1 activation, assayed via phosphorylation of 70S6K (RPS6KB1), 4EBP1 (EIF4EBP1) and/or S6 (RPS6)[39]. We do not find elevated phosphorylation of any of these targets in our PDGF-AA stimulated cells. In fact, we find that EIF4EBP2 phosphorylation is reduced. We also find no alteration to these canonical targets in ethanol-exposed cells. Three of the phospho-peptides enriched in the autophagy cluster, Stx7, Vamp8 and Snap29, are involved in fusion of the autophagosome and lyososome. Thus, it's likely that the effects of ethanol and PDGFRA are downstream or independent of mTORC1, which functions in the formation of the autophagosome.

Raptor is an essential component of mTORC1. In both mouse and zebrafish, loss of *Raptor* results in unregulated autophagy and craniofacial defects[32,40]. If Pdgfra signaling protects against runaway autophagy, then combined loss of Pdgfra and Raptor should exacerbate craniofacial defects. Indeed, we found that *pdgfra;raptor* double mutants have profound craniofacial defects more severe than either single

mutant. These double mutant phenotypes closely resemble those observed in ethanol-exposed *pdgfra* mutants, further supporting a role in autophagy for Pdgfra.

In developing organisms, a wide variety of environmental stressors can alter cellular homeostasis, effecting autophagy.[41] Ethanol is one of the most common environmental stressors of development. There is mixed literature regarding ethanol exposure and elevated autophagy. Ethanol reduces autophagy in cortical progenitor cells and neural crest cells differentiating into neurons.[42,43] In other cells (SH-SY5Y neuroblastoma cells and primary mouse microvascular endothelial cells), ethanol has been shown to elevate autophagy, but this is protective as elevating autophagy via mTOR inhibition protects against ethanol.[44,45] A similar protective role has been found in vivo during adrenal development.[46] We have found that elevated autophagy is deleterious. Some of these differences may be attributable to differences in cell types and exposure duration periods.[31] Here, we demonstrate in both mouse and human-derived neural crest cells that acute ethanol exposure elevates autophagy and that PDGFRA signaling ameliorates this effect and restores PDGF-AA dependent cell behaviors.

Ethanol disrupts Pdgfrα-dependent and independent cell migration

Pdgf signaling was first found to be essential for neural crest and craniofacial development in 1997.[9] Many years later, a role for Pdgfra signaling in neural crest cell migration was first demonstrated in zebrafish.[10] Soon afterwards, roles for Pdgfra signaling in neural crest cell migration were identified in mouse and *Xenopus.*[8,12] Here, we provide further support for a role of Pdgfra signaling in mouse neural crest cell migration and provide the new finding that PDGFRA signaling regulates neural crest cell migration in humans.

In iMEPM cells, we find that ethanol has no effect on the basal rate of cell migration but blunts migration in cells stimulated with PDGF-AA. A previous study did demonstrate an ethanol-induced reduction in the basal migratory rate of Joma1.3 cells, a cell line used to model neural crest cells.[47] This difference in findings likely reflects differences between the cell lines. The iMEPM cells were derived from mouse palatal mesenchyme, which would be post-migratory, while Joma1.3 cells were derived from trunk neural crest cells that had migrated away from the neural tube in culture.

Consistent with this difference, the iMEPM cells do not exhibit robust cell migration sans PDGF-AA stimulation which could make effects on the basal rate of migration difficult to detect. Human iPSCs differentiated into neural crest-like cells are highly migratory in the basal state. We find that PDGF-AA stimulation improves migration following ethanol exposure, demonstrating a role for PDGFRA function in human neural crest cell migration. Consistent with findings in the Joma1.3 cells, we find that ethanol reduces this basal rate of migration. Thus, migration appears to highly sensitive to environmental insult by ethanol.

Resource availability

Lead Contact

Further information and requests for resources and reagents should be directed to and will be fulfilled by the lead contact, Johann K. Eberhart (eberhart@austin.utexas.edu).

Materials availability

Zebrafish and cell lines used in this study are available from the lead contact upon reasonable request and completion of a materials transfer agreement.

Data and code availability

The raw data generated in this study are available upon reasonable request.

All original code and CellProfiler project have been deposited at https://github.com/shugesun/Pdgfra_ethanol_2026 and is publicly available as of the date of publication.

Acknowledgements

We gratefully thank Mary Swartz, Gissela Borrego-Soto, Josh Everson, Rayna Mazumdar, Alia Segura, Zoë Norton, Jaden Salganik, and Alpin Gunduz for their input and discussions during this project. We would like to thank Dr. Katherine Fantauzzo for generously providing iMEPM cells. We would like to thank UT core facilities for providing the Chemidoc MP Imaging System for immunoblot analysis. We would also like to thank Dr. Peter Faull from the Proteomics facility for the help with experiment design and set up, sample injection, and data acquisition for the phosphoproteomic analysis. We would like to thank Dickinson Lab and Chowdhury Lab for the help of cell

imaging. We thank Daniel Zepeda for assistance with the flow analysis. Finally, we thank the BME Core Facility for generously providing access to cell culture facilities at the early stages of this project.

Author contributions

S.S and J.K.E. conceived the study and designed the experiments. S.S. performed all experiments except: analyses in iPSCs and analyses of 10 vs 25 uM chloroquine, L.W.; migration assays in the *pdgfra* mutant zebrafish line, R.G.; *pdgfra;raptor* fish; S.K.T.; J.K.E. supervised analyses in iMEPM cells and in zebrafish; J.Z. supervised the iPSC work; S.S. and J.K.E. wrote the manuscript; all authors assisted in editing it.

Declaration of interests

The authors declare no competing interests.

Methods & Protocols

Key resources table

REAGENT or RESOURCE	**SOURCE**	**IDENTIFIER**
Antibody		
Anti-p-Pdgfra	Thermo Fisher Scientific	44-1006; RRID:AB_2533551
Anti-PDGFRA	Thermo Fisher Scientific	14-1401-82; RRID:AB_467491
Anti-p-AKT	Cell Signaling	4060S; RRID:AB_2315049
Anti-GAPDH	Abcam	ab210113; RRID:AB_3740832
Anti-Beta-tubulin	Cell Signaling	2146S; RRID:AB_2210545
Anti-MEF2C	Thermofisher	PA5-28247
Anti-HAND2	Thermofisher	H00009464-M03
PE-conjugated anti-CD271	Miltenyi Biotech	130-113-421
NucBlue Fixed Cell Stain ReadyProbes reagent	Invitrogen	R37606

Human TruStain FcX	BioLegend	422302
HRP conjugated goat anti-rabbit secondary antibody	Cell Signaling	7074S; RRID:AB_2099233
Alexa Fluor 488 conjugated goat anti-rabbit secondary antibody	Thermo Fisher Scientific	A11008; RRID:AB_143165
Anti-BrdU antibody	Bio-Rad Laboratories, Inc.	AHP2405; RRID:AB_2922993
Critical commercial assays		
HCR™ 2° IF kit	Molecular Instruments, Inc.	N/A
Experimental models: Cell lines		
iMEPM	Fantauzzo et al.[23]	RRID:CVCL_JX90
WTC11 hiPSC	Cellosaurus	GM25256
Experimental models: Organisms		
Zebrafish: *pdgfra*	Eberhart et al.[10]	RRID:ZFIN_ZDB-GENO-090112-4
Zebrafish: *pdgfra;raptor*	This paper	N/A
Chemicals, Peptides, and Recombinant Proteins		

PDGF-AA	R&D Systems	221-AA-025
DMEM	GIBCO	11995065
50 U/mL penicillin, 50 µg/mL streptomycin	GIBCO	15-140-122
L-glutamine	GIBCO	25-030-081
Neurobasal Media	Invitrogen	21103049
D-MEM F-12 Media	Invitrogen	11320033
B-27 Vitamin A	Invitrogen	A14700
N-2 (100x)	Invitrogen	S1049
bFGF	Peprotech	A1110501
bEGF	Sigma-Aldrich	46-034-CI
Fibronectin	Thermo Fisher	33016015
Bovine Insulin	Sigma-Aldrich	45000-436
BSA	Gemini Bio-Products	700-104P
100 Glutamax-I supplement	Invitrogen	35050061
CHIR-99021	Selleck/Tocris	S2924/8710
BMP2	Peprotech	120-02-50UG
0.5 EDTA, pH 8.0	Corning	46-034-CI
Essential 8 Medium, Basal	Thermo Fisher	A1517001
Vitronectin Recombinant Human Protein, Truncated	Thermo Fisher	A14700
ROCK Inhibitor (Y-27632)	Selleckchem	S1049
Accutase	Thermo Fisher	A1110501
Ethanol, 100%	Pharmco	111000200

Chloroquine diphosphate salt	Sigma-Aldrich	C6628-25G
CN03	Cytoskeleton, Inc.	CN03-A
CN04	Cytoskeleton, Inc.	CN04-A
BrdU	Abcam	ab142567
LysoTracker™ Red DND-99	Thermo Fisher Scientific	L7528
Hoechst	Thermo Fisher Scientific	62249
PBS	Thermo Fisher Scientific	10010072
DPBS	Thermo Fisher Scientific	14190144
Phenylmethylsulfonyl fluoride (PMSF)	Thermo Fisher Scientific	36978
Laemmli 2× sample buffer	Bio-Rad Laboratories, Inc.	1610737
8 M urea	Sigma-Aldrich	U5378-500G
Dithiothreitol (DTT)	Thermo Fisher Scientific	R0861
Halt protease and phosphatase inhibitor cocktails	Thermo Fisher Scientific	78442
β-mercaptoethanol	Thermo Fisher Scientific	31350010
RIPA buffer	Thermo Fisher Scientific	89900
TaqMan™ Fast Advanced Master Mix for qPCR	Thermo Fisher Scientific	4444963

MeltDoctor HRM Master Mix	Thermo Fisher Scientific	4415450
Oligonucleotides		
Primers for TaqMan SNP Genotyping Assays, see *DNA extraction and genotyping*	This paper	N/A
Primers for HRM assays, see *DNA extraction and genotyping*	This paper	N/A
Software and algorithms		
R v4.2.3	R Core Team	https://www.r-project.org/; RRID:SCR_001905
ComplexHeatmap v2.26.1	Gu et al. (2016)[48]; Gu (2022)[49]	https://bioconductor.org/packages/ComplexHeatmap/; RRID:SCR_017270
clusterProfiler v4.18.4	Yu[50]; Xu et al.[51]; Wu et al.[52]; Yu et al[53].	https://bioconductor.org/packages/release/bioc/html/clusterProfiler.html; RRID:SCR_016884
Tidyverse v2.0.0	Wickham et al.[54]	https://cran.r-project.org/web/packages/tidyverse/index.html; RRID:SCR_019186
FIJI v2.14.0	Schindelin et al.[55]	https://fiji.sc/; RRID:SCR_002285
CellProfiler 4.2.5	Broad Institute of MIT and Harvard	https://cellprofiler.org/; RRID:SCR_007358
Image Lab v6.1	Bio-Rad Laboratories, Inc.	https://www.bio-rad.com/en-us/product/image-lab-

		software?ID=KRE6P5E8Z/; RRID:SCR_014210
Graphpad Prism v8.3.1	GraphPad Software	https://www.graphpad.com/scientific-software/prism/; RRID:SCR_002798
Proteome Discoverer v2.2	Thermo Fisher Scientific	https://www.thermofisher.com/us/en/home/industrial/mass-spectrometry/liquid-chromatography-mass-spectrometry-lc-ms/lc-ms-software/multi-omics-data-analysis/proteome-discoverer-software.html/; RRID:SCR_014477
STRING v12.0	Szklarczyk et al.[29]	https://string-db.org/; RRID:SCR_005223

Method details

Cell culture

Immortalized mouse embryonic palatal mesenchymal (iMEPM) cells were generously donated by Dr. Katherine Fantauzzo.[23] Cells were cultured in DMEM (Dulbecco's modified Eagle's medium (GIBCO, Cat. No. 11995065) supplemented with 50 U/mL penicillin, 50 µg/mL streptomycin (GIBCO, Cat. No. 15-140-122) and 2 mM L-glutamine (GIBCO, Cat. No. 25-030-081) containing 10% FBS (fetal bovine serum, qualified; GIBCO, USA, Cat. No. 26-140-079) as previously described. Cells were grown on 10 cm^2 cell culture dishes (Thermo Fisher Scientific, Corning, Cell Culture, Treated, Nonpyrogenic, Polystyrene, Cat. No. 430167) to 90~100% cell confluency (~3.0×10^6) and split at a ratio of 1:5 for passages.

The WTC-11 hiPSC line (CelloSaurus, GM25256), was grown and expanded on vitronectin-coated plates (Thermo Fisher, Cat. No. A14700) in Essential 8 medium (Thermo Fisher, Cat. No. A1517001) to 80% confluence. The medium was changed daily, cells were split every 4-5 days with accutase (Thermo Fisher, Cat. No. A1110501) and plated with 10uM ROCK Inhibitor (Selleckchem, Cat. No. S1049) at a 1:5 dilution.

Cultures were routinely tested for mycoplasma using a Mycoplasma PCR Detection Kit (Abcam, Cat. No. ab289834).

HiPSCs were differentiated into CNCCs as previously described with some modifications[34]. Briefly, iPSCs were incubated with 0.5mM EDTA (Corning, Cat. No. 46-034-CI) for 8 minutes. Cells were washed once with DPBS (Cytiva, Cat. No. 45000-436) and then mechanically detached in clusters of 100-200 cells and plated in CNCC differentiation medium: 1:1 Neurobasal medium/D-MEM F-12 medium (Invitrogen Cat. Nos. 21103049 and 11320033), 0.5× B-27 supplement (50× stock, Invitrogen Cat. No. A14700), 0.5× N-2 supplement (100× stock, Invitrogen, Cat. No. S1049), 20 ng/ml bFGF (Peprotech, Cat. No. A1110501), 20 ng/ml EGF (Sigma-Aldrich, Cat. No. 46-034-CI), 5 µg/ml bovine insulin (Sigma-Aldrich, Cat. No. 45000-436) and 1× Glutamax-I supplement (100× stock, Invitrogen, Cat. No. 35050061). Medium was changed every other day. After nine days of differentiation, neuroepithelial spheres spontaneously attached to the dish and gave rise to the migratory CNCC population. Two to three days after the appearance of the first CNCC, neuroepithelial spheres were dissected away, and the migratory cell population was dissociated with accutase to single cells and passaged onto fibronectin-coated plates (Thermo Fisher, Cat. No. 33016015.) CNCCs were then transitioned to CNCC early maintenance media, which is composed of CNCC differentiation media substituting 1 mg/ml bovine serum albumin, serum replacement grade (Gemini Bio-Products # 700-104P) for bovine insulin. CNCCs were passaged onto fibronectin-coated plates 1:3 every three days, and after 2 passages, transitioned to CNCC long term maintenance media, which is composed of CNCC early maintenance media plus 3uM ChIRON 99021 (Selleck, CHIR-99021, Cat. No. S2924) and 50ng/ml BMP2 (Peprotech, Cat. No. 120-02-50UG).

Ethanol (Pharmco, 100%, Cat. No. 111000200) was diluted in DMEM containing 0.1% FBS for iMEPM cell treatment. Recombinant human PDGF-AA (R&D Systems, Cat. No. 221-AA-025) was reconstituted to a 5 µg/mL stock concentration with DMEM containing 0.1% FBS and further diluted to 10 or 30 ng/mL for treatment. Chloroquine (Chloroquine diphosphate salt, solid, ≥98%, Sigma-Aldrich, Cat. No. C6628-25G) was reconstituted to a 100 mM stock concentration with sterile water and diluted to 25/50/100/200 µM with DMEM containing 0.1% FBS for treatment.

Migration Assay

For iMEPM analyses, cells were seeded into a 6-well culture plate (Thermo Fisher Scientific, Fisherbrand, Cat. No. FB012927) and cultured to 100% confluency. Cells were then scratched with a P1000 pipet tip, washed with Phosphate Buffered Saline (PBS, Thermo Fisher Scientific, Cat. No. 10010072) and incubated in different treatments for 12 h with 5% CO_2 at 37℃. Cells were imaged using BioTek Cytation 5 cell imaging multi-mode reader (Agilent Technologies, Inc.). Migration distances were measured using FIJI.

HiPSC-derived CNCCs were seeded into a 24-well culture plate (Greiner Cellstar, Cat. No. 662160) and cultured to 100% confluency. Cells were then scratched with a P200 pipet tip, washed with DPBS and incubated in different treatments for 24 hours in an Incucyte (Sartorius, IncuCyte SX3) at 5% CO2 and at 37℃. Images were taken every 2 hours, and %Area of scratch without cells was measured using “Wound Healing” on FIJI (ImageJ).

Proliferation Assay

Cells at ~70% confluence grown on Slide Flasks (Thermo Fisher Scientific, Nunc, Lab-Tek, Cat. No. 12-565-112) were serum-starved overnight in medium containing 0.1% FBS and incubated with different treatments for 24 hours with 5% CO_2 at 37℃. After PBS washes, cells were then incubated with 0.1% FBS DMEM containing 10 μM BrdU (5-bromo-2’-deoxyuridine, Abcam. Cat. No. ab142567) for 1 hour with 5% CO_2 at 37℃. Cells were fixed with 4% PFA (paraformaldehyde) for 10 min at RT, and then permeabilized with 0.2% Triton X-100 for 10 min at RT. Cells were treated with1.5 M HCl for 30 min at RT to denature DNA. After 3 PBS washes, cells were incubated with 5% non-fat milk for 1 hour at RT. Rabbit anti-BrdU antibody (Bio-Rad Laboratories, Inc., Cat. No. AHP2405) was diluted (1:250) in PBST (0.1% Tween 20 in PBS) and incubated for 1 hour at RT. Followed by 3x PBST washes, Alexa Fluor 488 conjugated goat anti-rabbit IgG secondary antibody (Thermo Fisher Scientific, Invitrogen, Cat. No. A11008) was diluted 1:200 in PBST and incubated for 1 hour at RT in the dark. Cells were counterstained with DAPI and incubated at RT for 10 min. Images were taken using a Zeiss LSM 980 confocal microscope. The ratio of BrdU-positive cells to total

cells was calculated using CellProfiler. The CellProfiler .cpproj is provided at https://github.com/shugesun/Pdgfra_ethanol_2026.

HCR™ immunofluorescence

A detailed protocol is described on Molecular Instrument website (https://www.molecularinstruments.com/). HCR™ 2° IF kit was used. Briefly, after sample preparation and blocking, immunodetection was performed using a phosphorylated Pdgfra(p-PDGFRα) primary antibody diluted in HCR™ Antibody Buffer (provided in the kit) overnight. Slides were washed by immersing in PBST at room temperature for 3 × 5 min. Cells were incubated with an HCR™ secondary Antibody Probe (provided in the kit) at 1 μg/mL in HCR™ Antibody Buffer. HCR hairpins B1H1 488 and B1H2 488 were used at the amplification stage.

Phospho-Proteomic Analysis

This method was adapted from the EasyPhos platform, and all chemicals used prior to injections are described in Humphrey et al.[26] For each treatment, 200 μg protein was prepared per sample and 4 replicates for each treatment were processed and analyzed. Samples were injected into a Thermo Orbitrap Fusion hybrid mass spectrometer (provided by UT Proteomics Core Facility). Data was processed by Proteome Discoverer™ 2.2 Software (Thermo Fisher Scientific) and R (R codes are provided in the Supplemental information).

RNA-Sequencing of iMEPM cells

iMEPM cells were cultured in 10-cm dishes and serum-starved overnight prior to treatment. Cells were treated with 1% ethanol for 1 h, while control cells were maintained under identical conditions without ethanol. Five independent biological replicates were collected for each condition.

Total RNA was isolated using the RNeasy Mini Kit (QIAGEN, Cat. No. 74104) according to the manufacturer's instructions. Cells were lysed directly in the culture dishes using 600 μL Buffer RLT supplemented with β-mercaptoethanol and homogenized. An equal volume of 70% ethanol was added to each homogenized lysate and mixed thoroughly before application to RNeasy spin columns. Columns were subsequently washed with Buffer RW1 and Buffer RPE, and purified RNA was eluted in

RNase-free water. RNA concentration and purity were assessed using a NanoDrop spectrophotometer, and RNA samples were stored at −80°C until sequencing.

The GSAF at UT Austin Tag-seq performed library preparation and sequencing. Sequencing reads were aligned to the Mus musculus GRCm39 reference genome and gene-level read counts were used for downstream differential-expression analysis performed on https://ranaseq.eu/.[56]

Lysotracker Staining

Cells were incubated with 50 LysoTracker™ Red DND-99 (Thermo Fisher Scientific, Invitrogen, Cat. No. L7528) together with 20 μM Hoechst (Thermo Fisher Scientific, Invitrogen, Cat. No. 62249) diluted in 0.1% FBS DMEM for 5 (iMEPM) or diluted in CNCC long term maintenance media for 60 minutes (hiPSC-CNCCs) and then washed with Dulbecco's phosphate-buffered saline (DPBS, Thermo Fisher Scientific, Gibco, Cat. No. 14190144). Images were taken using a Zeiss LSM 980 Confocal Microscope. Autophagy was measured by obtaining %area of LysoTracker Deep Red signal using FIJI (ImageJ) and divided by the number of cells. Analyses were performed in triplicate.

CNCC Immunofluorescence

CNCCs were plated on glass bottom plates (Cellvis, NC0397150) coated in fibronectin (Thermo Fisher, Cat. No. 33016015) and grown until 60-80% confluent (2 days). They were then fixed in 4% PFA, permeabilized with 0.3% Triton-X 100, and blocked with 1% BSA PBST for one hour. Primary antibodies were diluted in 1% BSA PBST and incubated overnight at 4C. Primary antibodies include: MEF2C (1:250, Thermofisher, PA5-28247) and HAND2 (1:50, Thermofisher H00009464-M03). Afterward, the cells were washed 3 times with DPBS and incubated covered at room temperature for 45 minutes with fluorophore-conjugated secondary antibodies diluted 1:1000 in PBST: Alexa Fluor 488 goat-anti rabbit (Invitrogen, A27034SAMPL) Alexa Fluor 633 goat-anti mouse (Invitrogen, 21126). Cells were washed again with PBS, then nuclei were stained with NucBlue Fixed Cell Stain Ready Probes reagent (Invitrogen, R37606) was added for 7 minutes before final washing with PBS. Images were taken using Leica DMi8 Confocal Microscopy. Images of five random fields were taken for each sample; images are representative.

Fluorescence-activated cell sorting (FACS)

FACS buffer was prepared with 2mM EDTA and 0.5% BSA diluted in DPBS. Cells were washed once with DPBS, collected via actutase, and spun down for 5 minutes at 300xg. They were then resuspended in 100ul of FACS buffer with 5ul of Human TruStain FcX block (BioLegend, 422302) and incubated at room temperature for 10 minutes. PE-conjugated anti-CD271 was added (1:100, Miltenyi Biotec 130-113-421) and the cell suspension was incubated for 30 minutes at 4C. After incubation, 1.9 ml of more FACS buffer was added, and the cells were passed through a cell strainer twice before sorting via the Sony MA900. Debris was excluded using forward and side scatter area, and gating was guided via fluorescence intensity. Viable CD271+ cells were sorted in CNCC media and replated on fibronectin coated plates. Analysis was performed using FlowJo.

***Danio rerio* (zebrafish) care and use**

Zebrafish were raised and cared for using established protocols[57] with IACUC approval from the University of Texas at Austin. Embryos were collected from natural mating and raised in embryo medium (EM) under standard laboratory conditions. For experimental treatments, embryos were exposed to 1% ethanol (Pharmco, 100%, Cat. No. 111000200, diluted with EM) at the indicated developmental stages. Chloroquine (Chloroquine diphosphate salt, solid, ≥98%, Sigma-Aldrich, Cat. No. C6628-25G) was reconstituted to a 100 mM stock concentration with sterile water, diluted to 1.5 mM with EM, and treated at the indicated developmental stages. CN03 (Cytoskeleton, Inc., Cat. No. CN03-A) and CN04 (Cytoskeleton, Inc., Cat. No. CN04-A) were reconstitute to 100 µg/mL with sterile water and diluted to a final concentration of 1 µg/mL with EM for treatment. The *pdgfra*^{b1059} and *raptor*^{au93} mutant alleles[10] were used for genetic analyses in this study. Embryos were staged according to established morphological criteria[58].

Alcian and Alizarin Staining

To assess craniofacial cartilage and bone development, four days post-fertilization (4 dpf) zebrafish larvae were stained with Alcian Blue and Alizarin Red as previously described.[59] Briefly, larvae were processed to allow differential visualization of cartilage (Alcian Blue) and mineralized bone (Alizarin Red).

After completion of staining and clearing, specimens were mounted and imaged using a Zeiss Axio Imager-A1 microscope. Morphometric measurements were performed using AxiovisionLE software (AxioVs40 V4.7.1.0). All measurements were conducted using consistent anatomical landmarks across specimens to ensure reproducibility.

Quantitative data were compiled using GraphPad Prism version 8.3.1. Statistical analyses were performed using analysis of variance (ANOVA) for all comparisons. Data are presented as mean ± SEM, and statistical significance was determined using appropriate post hoc tests as indicated.

Immunoblotting

IMEPM cells

Cells at ~80% confluence were serum-starved overnight in medium containing 0.1% FBS and incubated with different treatments for the indicated length of time. At the end of treatment, cells were harvested in ice-cold lysis buffer (Cell Signaling Technology, Inc., Danvers, MA, USA. Cat. No. 9803) supplemented with 1 mM phenylmethylsulfonyl fluoride (PMSF, Thermo Fisher Scientific, Cat. No. 36978). Cells were incubated on ice for 5 min before scraping. Total cell lysates were sonicated briefly and then collected by centrifugation at 14,000× g for 10 min at 4 ℃.

For sodium dodecyl sulfate-polyacrylamide gel electrophoresis (SDS-PAGE), protein samples were mixed 1:1 (v/v) with Laemmli 2× sample buffer (Bio-Rad Laboratories, Inc., Cat. No. 1610737) supplemented with 8 M urea (Sigma-Aldrich, Cat. No. U5378-500G), 1mM dithiothreitol (DTT, Thermo Fisher Scientific, Cat. No. R0861), 1× Halt protease and phosphatase inhibitor cocktails (PPI, Thermo Fisher Scientific, Cat. No. 78442), and 10% by volume β-mercaptoethanol (BME, Thermo Fisher Scientific, Cat. No. 31350010). Samples were denatured by heating at 95 °C for 5 min.

Zebrafish

Zebrafish larvae were euthanized at 4 dpf according to approved protocols, and heads were dissected by transection at the midbrain–hindbrain boundary to enrich for craniofacial tissues. For each experimental condition, 7-8 heads were pooled into a single microcentrifuge tube to obtain sufficient protein for immunoblot analysis.

Samples were lysed on ice in 350 µL RIPA buffer (Thermo Fisher Scientific, Cat. No. 89900) containing 10 mM PMSF (Thermofisher Scientific, Cat. No. 36978), 1× Halt PPI (Thermo Fisher Scientific, Cat. No. 78442), and 10% BME (Thermo Fisher Scientific, Cat. No. 31350010).

Head lysates were sonicated three times for 30 s each with 15 s intervals to disrupt tissue and reduce viscosity, followed by clarification via centrifugation at 14,000 × g for 10 min at 4 °C. The resulting supernatants were collected as whole-head protein extracts for downstream analysis. For SDS-PAGE, protein samples were mixed 1:1 (v/v) with Laemmli 2× sample buffer (Bio-Rad Laboratories, Inc., Cat. No. 1610737) supplemented with an additional 10% BME (Thermo Fisher Scientific, Cat. No. 31350010), and denatured by heating at 95 °C for 5 min.

Proteins collected from both models were resolved by SDS-PAGE using 4-20% Mini-PROTEAN® TGX™ Precast protein Gels (10-well, 50 µL; Bio-Rad Laboratories, Inc., Cat. No. 4561094). Following electrophoresis, proteins were transferred to PVDF membranes (Bio-Rad Laboratories, Inc., Cat. No. 1704272) using standard immunoblotting procedures. Membranes were probed with primary and secondary antibodies as indicated; detailed antibody information is provided in **Key resources table**. Immunoreactive bands were detected by Chemidoc MP Imaging System (Bio-Rad Laboratories, Inc., Cat. No. 12003154) and quantified using Image Lab software (Image Lab 6.1; Bio-Rad Laboratories, Inc.). Signal intensities were measured within the linear range of detection and normalized as described in the corresponding figure legends and texts.

DNA extraction and genotyping

Genomic DNA was extracted from zebrafish tail tissue following standard protocols. Briefly, tail clips were collected and processed to isolate genomic DNA suitable for downstream genotyping analyses.

Genotyping for *pdgfra* gene was performed using TaqMan™ SNP Genotyping Assays (Thermo Fisher Scientific), which enable allele-specific discrimination through fluorescent reporter probes. Assays were designed to distinguish the *pdgfra*^{b1059} mutant allele from the wild-type allele. TaqMan™ Fast Advanced Master Mix for qPCR (Thermo Fisher Scientific, Cat. No. 4444963) was used as the master mix.

For the TaqMan assay, the following primer and probe sequences were used to identify *pdgfra* genotype: a forward primer (CGCTGAGTGATGTCTGGTCTTA), a reverse primer (TGAAACATACCGAGAGAGAAGAT), reporter 1 probe (CTCCCATAATAAGATGCCA), and reporter 2 probe (CTCCCATAATAAGTTGCCA). The context sequence used for SNP discrimination was CTGAGTGATGTCTGGTCTTATGGCA[T/A]CTTATTATGGGAGATCTTCTCTCTC, where the bracketed nucleotide denotes the wild-type or mutant allele.

Genotype calls were assigned based on allele-specific fluorescence signals according to the manufacturer's instructions. All genotyping reactions included appropriate controls to ensure accurate allele discrimination.

Genotyping for *raptor* gene was performed using High-Resolution Melting (HRM) analysis with a forward primer (TTTCATCGAGGGAGGCA), a reverse primer (TTCATCGAGGGAGGCAGA), and MeltDoctor HRM Master Mix (Thermo Fisher Scientific, Cat. No. 4415450).

References

1. Couly, G.F., Coltey, P.M., and Le Douarin, N.M. (1993). The triple origin of skull in higher vertebrates: a study in quail-chick chimeras. Development *117*, 409-429. 10.1242/dev.117.2.409.
2. Evans, D.J., and Noden, D.M. (2006). Spatial relations between avian craniofacial neural crest and paraxial mesoderm cells. Dev Dyn *235*, 1310-1325. 10.1002/dvdy.20663.
3. Santagati, F., and Rijli, F.M. (2003). Cranial neural crest and the building of the vertebrate head. Nat Rev Neurosci *4*, 806-818. 10.1038/nrn1221.
4. Le Lievre, C.S. (1978). Participation of neural crest-derived cells in the genesis of the skull in birds. J Embryol Exp Morphol *47*, 17-37.
5. Theveneau, E., and Mayor, R. (2012). Neural crest delamination and migration: from epithelium-to-mesenchyme transition to collective cell migration. Dev Biol *366*, 34-54. 10.1016/j.ydbio.2011.12.041.
6. Bush, J.O., and Jiang, R. (2012). Palatogenesis: morphogenetic and molecular mechanisms of secondary palate development. Development *139*, 231-243. 10.1242/dev.067082.
7. Dixon, M.J., Marazita, M.L., Beaty, T.H., and Murray, J.C. (2011). Cleft lip and palate: understanding genetic and environmental influences. Nat Rev Genet *12*, 167-178. 10.1038/nrg2933.
8. Bahm, I., Barriga, E.H., Frolov, A., Theveneau, E., Frankel, P., and Mayor, R. (2017). PDGF controls contact inhibition of locomotion by regulating N-cadherin during neural crest migration. Development *144*, 2456-2468. 10.1242/dev.147926.
9. Soriano, P. (1997). The PDGF alpha receptor is required for neural crest cell development and for normal patterning of the somites. Development *124*, 2691-2700. 10.1242/dev.124.14.2691.
10. Eberhart, J.K., He, X., Swartz, M.E., Yan, Y.L., Song, H., Boling, T.C., Kunerth, A.K., Walker, M.B., Kimmel, C.B., and Postlethwait, J.H. (2008). MicroRNA Mirn140 modulates Pdgf signaling during palatogenesis. Nat Genet *40*, 290-298. 10.1038/ng.82.
11. Tallquist, M.D., and Soriano, P. (2003). Cell autonomous requirement for PDGFRalpha in populations of cranial and cardiac neural crest cells. Development *130*, 507-518. 10.1242/dev.00241.
12. He, F., and Soriano, P. (2013). A critical role for PDGFRalpha signaling in medial nasal process development. PLoS Genet *9*, e1003851. 10.1371/journal.pgen.1003851.
13. McCarthy, N., Wetherill, L., Lovely, C.B., Swartz, M.E., Foroud, T.M., and Eberhart, J.K. (2013). Pdgfra protects against ethanol-induced craniofacial defects in a zebrafish model of FASD. Development *140*, 3254-3265. 10.1242/dev.094938.
14. Yu, Y., Alvarado, R., Petty, L.E., Bohlender, R.J., Shaw, D.M., Below, J.E., Bejar, N., Ruiz, O.E., Tandon, B., Eisenhoffer, G.T., et al. (2022). Polygenic risk impacts PDGFRA mutation penetrance in non-syndromic cleft lip and palate. Hum Mol Genet *31*, 2348-2357. 10.1093/hmg/ddac037.
15. Diaz Perez, K.K., Curtis, S.W., Sanchis-Juan, A., Zhao, X., Head, T., Ho, S., Carter, B., McHenry, T., Bishop, M.R., Valencia-Ramirez, L.C., et al. (2023). Rare variants found in clinical gene panels illuminate the genetic and allelic architecture of orofacial clefting. Genet Med *25*, 100918. 10.1016/j.gim.2023.100918.

16. Yu, X., Yang, S., Xia, W., Zhou, X., Gao, M., Shi, H., and Zhou, Y. (2023). Identification of a Novel Variant of PDGFC Associated with Nonsyndromic Cleft Lip and Palate in a Chinese Family. Int J Genomics *2023*, 8814046. 10.1155/2023/8814046.
17. Smith, S.M., Garic, A., Flentke, G.R., and Berres, M.E. (2014). Neural crest development in fetal alcohol syndrome. Birth Defects Res C Embryo Today *102*, 210-220. 10.1002/bdrc.21078.
18. Sulik, K.K. (2005). Genesis of alcohol-induced craniofacial dysmorphism. Exp Biol Med (Maywood) *230*, 366-375. 10.1177/15353702-0323006-04.
19. Klingenberg, C.P., Wetherill, L., Rogers, J., Moore, E., Ward, R., Autti-Ramo, I., Fagerlund, A., Jacobson, S.W., Robinson, L.K., Hoyme, H.E., et al. (2010). Prenatal alcohol exposure alters the patterns of facial asymmetry. Alcohol *44*, 649-657. 10.1016/j.alcohol.2009.10.016.
20. Lovely, C.B., Fernandes, Y., and Eberhart, J.K. (2016). Fishing for Fetal Alcohol Spectrum Disorders: Zebrafish as a Model for Ethanol Teratogenesis. Zebrafish *13*, 391-398. 10.1089/zeb.2016.1270.
21. Kanshin, E., Bergeron-Sandoval, L.P., Isik, S.S., Thibault, P., and Michnick, S.W. (2015). A cell-signaling network temporally resolves specific versus promiscuous phosphorylation. Cell Rep *10*, 1202-1214. 10.1016/j.celrep.2015.01.052.
22. Jiang, W., Jaehnig, E.J., Liao, Y., Shi, Z., Yaron-Barir, T.M., Johnson, J.L., Cantley, L.C., and Zhang, B. (2025). Deciphering the dark cancer phosphoproteome using machine-learned co-regulation of phosphosites. Nat Commun *16*, 2766. 10.1038/s41467-025-57993-2.
23. Fantauzzo, K.A., and Soriano, P. (2017). Generation of an immortalized mouse embryonic palatal mesenchyme cell line. PLoS One *12*, e0179078. 10.1371/journal.pone.0179078.
24. Yu, J., Deuel, T.F., and Kim, H.R. (2000). Platelet-derived growth factor (PDGF) receptor-alpha activates c-Jun NH2-terminal kinase-1 and antagonizes PDGF receptor-beta -induced phenotypic transformation. J Biol Chem *275*, 19076-19082. 10.1074/jbc.M910329199.
25. Fantauzzo, K.A., and Soriano, P. (2014). PI3K-mediated PDGFRalpha signaling regulates survival and proliferation in skeletal development through p53-dependent intracellular pathways. Genes Dev *28*, 1005-1017. 10.1101/gad.238709.114.
26. Humphrey, S.J., Karayel, O., James, D.E., and Mann, M. (2018). High-throughput and high-sensitivity phosphoproteomics with the EasyPhos platform. Nat Protoc *13*, 1897-1916. 10.1038/s41596-018-0014-9.
27. Doanes, A.M., Irani, K., Goldschmidt-Clermont, P.J., and Finkel, T. (1998). A requirement for rac1 in the PDGF-stimulated migration of fibroblasts and vascular smooth cells. Biochem Mol Biol Int *45*, 279-287. 10.1080/15216549800202652.
28. Van Aelst, L., and D'Souza-Schorey, C. (1997). Rho GTPases and signaling networks. Genes Dev *11*, 2295-2322. 10.1101/gad.11.18.2295.
29. Szklarczyk, D., Kirsch, R., Koutrouli, M., Nastou, K., Mehryary, F., Hachilif, R., Gable, A.L., Fang, T., Doncheva, N.T., Pyysalo, S., et al. (2023). The STRING database in 2023: protein-protein association networks and functional enrichment analyses for any sequenced genome of interest. Nucleic Acids Res *51*, D638-D646. 10.1093/nar/gkac1000.

30. Behrends, C., Sowa, M.E., Gygi, S.P., and Harper, J.W. (2010). Network organization of the human autophagy system. Nature *466*, 68-76. 10.1038/nature09204.
31. Tucker, S.K., and Eberhart, J.K. (2024). The convergence of mTOR signaling and ethanol teratogenesis. Reprod Toxicol *130*, 108720. 10.1016/j.reprotox.2024.108720.
32. Tucker, S.K., Ghosal, R., Swartz, M.E., Zhang, S., and Eberhart, J.K. (2024). Zebrafish raptor mutation inhibits the activity of mTORC1, inducing craniofacial defects due to autophagy-induced neural crest cell death. Development *151*. 10.1242/dev.202216.
33. Chen, J., Yao, Y., Wang, X., Wang, Y., Li, T., and Du, J. (2022). Chloroquine regulates the proliferation and apoptosis of palate development on mice embryo by activating P53 through blocking autophagy in vitro. In Vitro Cell Dev Biol Anim *58*, 558-570. 10.1007/s11626-022-00704-8.
34. Prescott, S.L., Srinivasan, R., Marchetto, M.C., Grishina, I., Narvaiza, I., Selleri, L., Gage, F.H., Swigut, T., and Wysocka, J. (2015). Enhancer divergence and cis-regulatory evolution in the human and chimp neural crest. Cell *163*, 68-83. 10.1016/j.cell.2015.08.036.
35. Dossou, A.S., and Basu, A. (2019). The Emerging Roles of mTORC1 in Macromanaging Autophagy. Cancers (Basel) *11*. 10.3390/cancers11101422.
36. Simpson, J.E., and Gammoh, N. (2024). Autophagy cooperates with PDGFRA to support oncogenic growth signaling. Autophagy *20*, 1901-1902. 10.1080/15548627.2024.2338572.
37. Simpson, J.E., Muir, M.T., Lee, M., Naughton, C., Gilbert, N., Pollard, S.M., and Gammoh, N. (2024). Autophagy supports PDGFRA-dependent brain tumor development by enhancing oncogenic signaling. Dev Cell *59*, 228-243 e227. 10.1016/j.devcel.2023.11.023.
38. Inoki, K., Li, Y., Zhu, T., Wu, J., and Guan, K.L. (2002). TSC2 is phosphorylated and inhibited by Akt and suppresses mTOR signalling. Nat Cell Biol *4*, 648-657. 10.1038/ncb839.
39. Sapi, Z., Fule, T., Hajdu, M., Matolcsy, A., Moskovszky, L., Mark, A., Sebestyen, A., and Bodoky, G. (2011). The activated targets of mTOR signaling pathway are characteristic for PDGFRA mutant and wild-type rather than KIT mutant GISTs. Diagn Mol Pathol *20*, 22-33. 10.1097/PDM.0b013e3181eb931b.
40. Nie, X., Zheng, J., Ricupero, C.L., He, L., Jiao, K., and Mao, J.J. (2018). mTOR acts as a pivotal signaling hub for neural crest cells during craniofacial development. PLoS Genet *14*, e1007491. 10.1371/journal.pgen.1007491.
41. Lei, J., Calvo, P., Vigh, R., and Burd, I. (2018). Journey to the Center of the Fetal Brain: Environmental Exposures and Autophagy. Front Cell Neurosci *12*, 118. 10.3389/fncel.2018.00118.
42. Prock, T.L., and Miranda, R.C. (2007). Embryonic cerebral cortical progenitors are resistant to apoptosis, but increase expression of suicide receptor DISC-complex genes and suppress autophagy following ethanol exposure. Alcohol Clin Exp Res *31*, 694-703. 10.1111/j.1530-0277.2007.00354.x.
43. Fan, H., Yuan, F., Yun, Y., Wu, T., Lu, L., Liu, J., Feng, W., and Chen, S.Y. (2019). MicroRNA-34a mediates ethanol-induced impairment of neural differentiation of neural crest cells by targeting autophagy-related gene 9a. Exp Neurol *320*, 112981. 10.1016/j.expneurol.2019.112981.

44. Chen, G., Ke, Z., Xu, M., Liao, M., Wang, X., Qi, Y., Zhang, T., Frank, J.A., Bower, K.A., Shi, X., and Luo, J. (2012). Autophagy is a protective response to ethanol neurotoxicity. Autophagy *8*, 1577-1589. 10.4161/auto.21376.
45. Girault, V., Gilard, V., Marguet, F., Lesueur, C., Hauchecorne, M., Ramdani, Y., Laquerriere, A., Marret, S., Jegou, S., Gonzalez, B.J., et al. (2017). Prenatal alcohol exposure impairs autophagy in neonatal brain cortical microvessels. Cell Death Dis *8*, e2610. 10.1038/cddis.2017.29.
46. Huang, H., Liu, L., Li, J., Zhu, C., Xie, X., Ao, Y., and Wang, H. (2018). Autophagy as a compensation mechanism participates in ethanol-induced fetal adrenal dysfunction in female rats. Toxicol Appl Pharmacol *345*, 36-47. 10.1016/j.taap.2018.03.007.
47. Fan, H., Li, Y., Yuan, F., Lu, L., Liu, J., Feng, W., Zhang, H.G., and Chen, S.Y. (2022). Up-regulation of microRNA-34a mediates ethanol-induced impairment of neural crest cell migration in vitro and in zebrafish embryos through modulating epithelial-mesenchymal transition by targeting Snail1. Toxicol Lett *358*, 17-26. 10.1016/j.toxlet.2022.01.004.
48. Gu, Z., Eils, R., and Schlesner, M. (2016). Complex heatmaps reveal patterns and correlations in multidimensional genomic data. Bioinformatics *32*, 2847-2849. 10.1093/bioinformatics/btw313.
49. Gu, Z. (2022). Complex heatmap visualization. Imeta *1*, e43. 10.1002/imt2.43.
50. Yu, G. (2024). Thirteen years of clusterProfiler. Innovation (Camb) *5*, 100722. 10.1016/j.xinn.2024.100722.
51. Xu, S., Hu, E., Cai, Y., Xie, Z., Luo, X., Zhan, L., Tang, W., Wang, Q., Liu, B., Wang, R., et al. (2024). Using clusterProfiler to characterize multiomics data. Nat Protoc *19*, 3292-3320. 10.1038/s41596-024-01020-z.
52. Wu, T., Hu, E., Xu, S., Chen, M., Guo, P., Dai, Z., Feng, T., Zhou, L., Tang, W., Zhan, L., et al. (2021). clusterProfiler 4.0: A universal enrichment tool for interpreting omics data. Innovation (Camb) *2*, 100141. 10.1016/j.xinn.2021.100141.
53. Yu, G., Wang, L.G., Han, Y., and He, Q.Y. (2012). clusterProfiler: an R package for comparing biological themes among gene clusters. OMICS *16*, 284-287. 10.1089/omi.2011.0118.
54. Wickham, H.A., M.; Bryan, J.; Chang, W.; McGowan, L. D.; François, R.; Grolemund, G.; Hayes, A.; Henry, L.; Hester, J.; Kuhn, M.; Pedersen, T. L.; Miller, E.; Bache, S. M.; Müller, K.; Ooms, J.; Robinson, D.; Seidel, D. P.; Spinu, V.; Takahashi, K.; Vaughan D, Wilke C, Woo K, Yutani, H. (2019). Welcome to the tidyverse. Journal of Open Source Software *4*.
55. Schindelin, J., Arganda-Carreras, I., Frise, E., Kaynig, V., Longair, M., Pietzsch, T., Preibisch, S., Rueden, C., Saalfeld, S., Schmid, B., et al. (2012). Fiji: an open-source platform for biological-image analysis. Nat Methods *9*, 676-682. 10.1038/nmeth.2019.
56. Prieto, C., and Barrios, D. (2019). RaNA-Seq: Interactive RNA-Seq analysis from FASTQ files to functional analysis. Bioinformatics. 10.1093/bioinformatics/btz854.
57. Westerfield, M. (1993). The Zebrafish Book: A Guide For the Laboratory Use of Zebrafish (Brachydanio Rerio). Eugene, OR: University of Oregon Press.
58. Kimmel, C.B., Ballard, W.W., Kimmel, S.R., Ullmann, B., and Schilling, T.F. (1995). Stages of embryonic development of the zebrafish. Dev Dyn *203*, 253-310. 10.1002/aja.1002030302.

59. Walker, M.B., and Kimmel, C.B. (2007). A two-color acid-free cartilage and bone stain for zebrafish larvae. Biotech Histochem *82*, 23-28. 10.1080/10520290701333558.

Figures

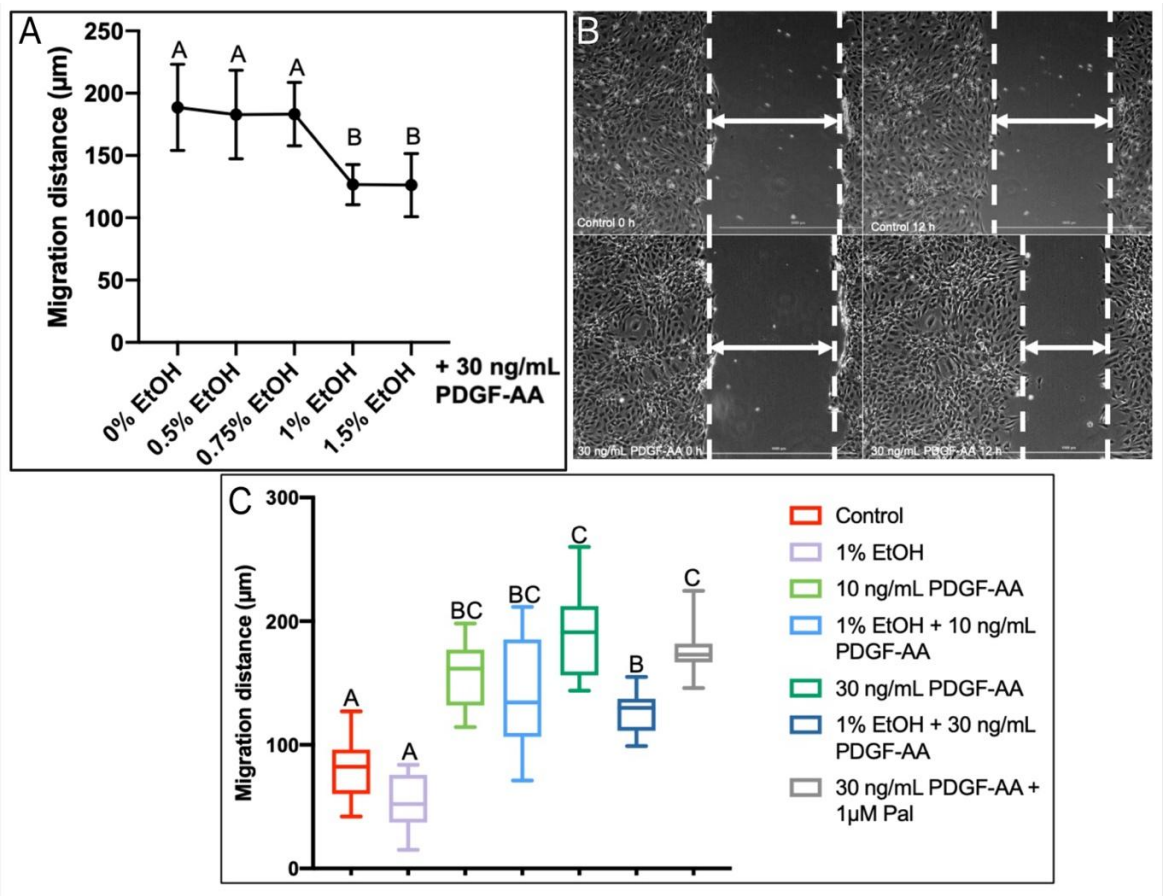


Figure 1. Ethanol treatment inhibits PDGF-AA–induced iMEPM migration.
(A) Dose–response analysis of ethanol (EtOH) revealed that 1% is the threshold concentration that impairs cell migration (error bars represent SD). (B) Representative scratch assay images show how the gap width changed during treatment for control and 30 ng/mL PDGF-AA. Migration distance was calculated as the difference in gap width between the two time points. (C) Quantification of migration distances across treatment groups (one-way ANOVA, *n* = 12 per group; error bars represent SD; groups that share the same letter are not significantly different from one another). PDGF-AA treatment significantly promoted cell migration compared with control, but this effect was attenuated when ethanol was present. The group treated with PDGF-AA and the proliferation inhibitor palbociclib (Pal) displayed migration distances comparable to PDGF-AA alone, confirming that changes in wound closure were due to cell migration rather than proliferation. EtOH: ethanol; Pal: palbociclib.

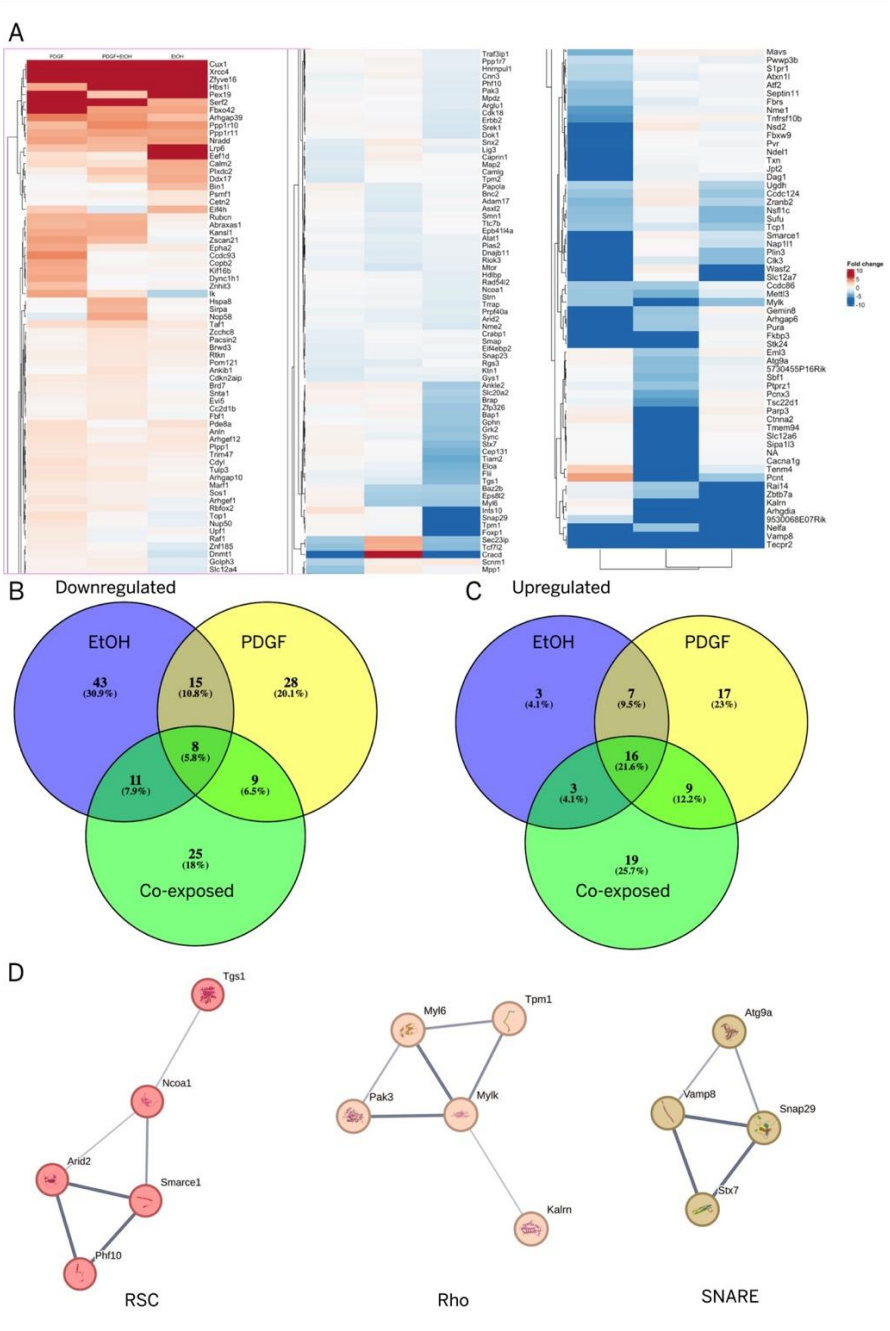


Figure 2. Differentially expressed phosphoproteins across PDGF-AA, EtOH, and combined treatments. (A) Hierarchical clustering of all significantly altered phosphoproteins found in the phosphoproteomic dataset is shown for three comparisons: PDGF-AA vs control, PDGF-AA + EtOH vs control, and EtOH vs control. Fold changes are shown on a red–blue color scale. (B, C) Venn diagram displaying overlapping differentially expressed downregulated (B) and upregulated (C) phosphoproteins. (D) Top 3 clusters identified in STRING analysis.

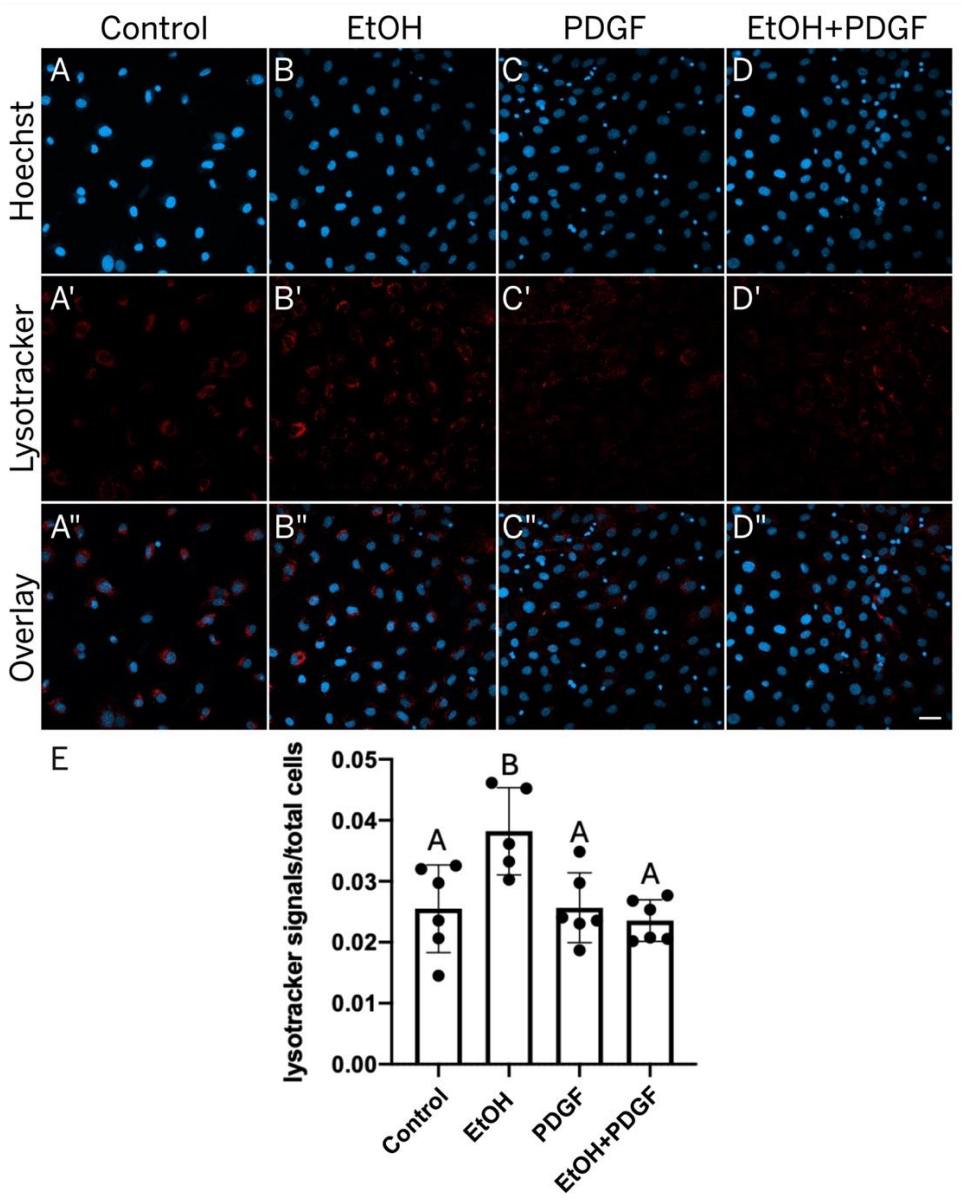


Figure 3. Ethanol treatment elevates autophagy in iMEPM cells.

(A–D) Representative Lysotracker staining after 60 min incubation. Ethanol-treated cells exhibited significantly higher autophagic activity compared with other groups, consistent with the phospho-proteomic results. Notably, co-treatment with PDGF-AA reduced ethanol-induced autophagy to control levels, effectively rescuing the phenotype. (E) Quantification of Lysotracker fluorescence intensity across groups (one-way ANOVA, $n \geq 5$ per group; Groups that share a letter are not statistically significant from one another.; error bars represent SD). EtOH: ethanol.

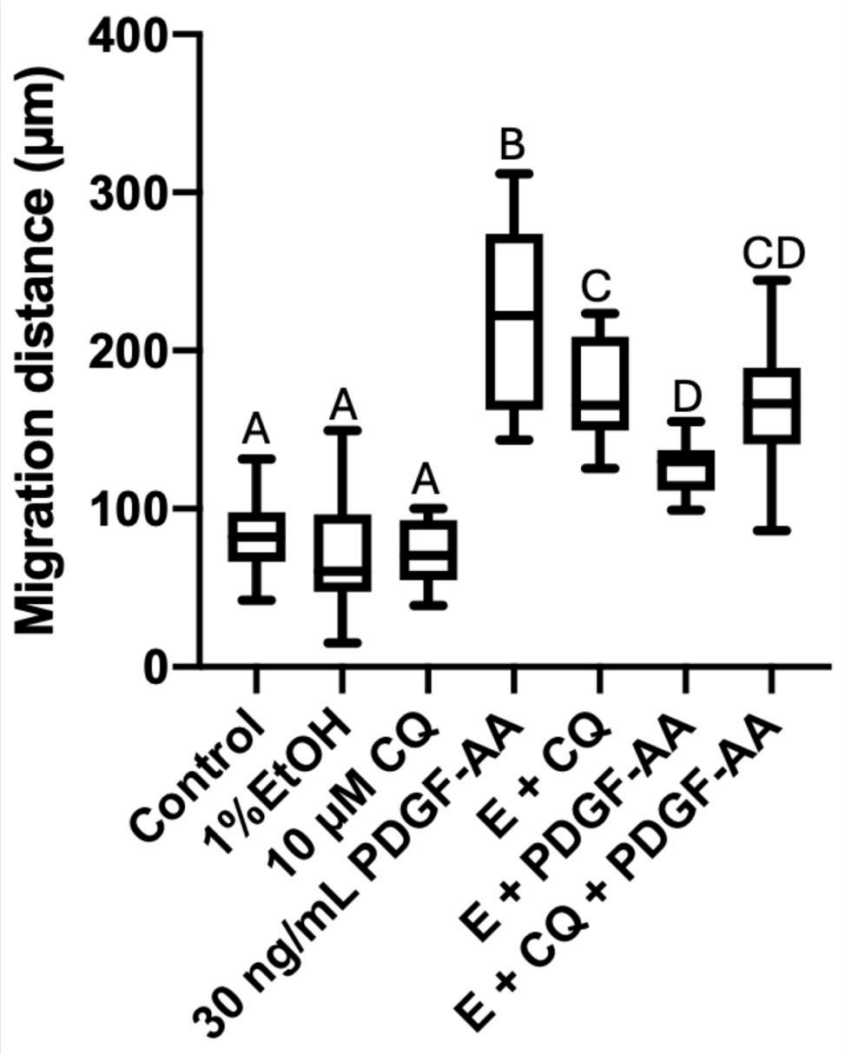


Figure 4. Inhibiting autophagy restores cell migration. Chloroquine treatment (CQ, 10 µM) elevated migration in ethanol-treated cells compared with ethanol (EtOH) alone. PDGF-AA stimulation improved migration in ethanol-exposed cells, relative to ethanol alone (one-way ANOVA, $n \geq 12$ per group; error bars represent SD, Groups that share a letter are not statistically significant from one another.).

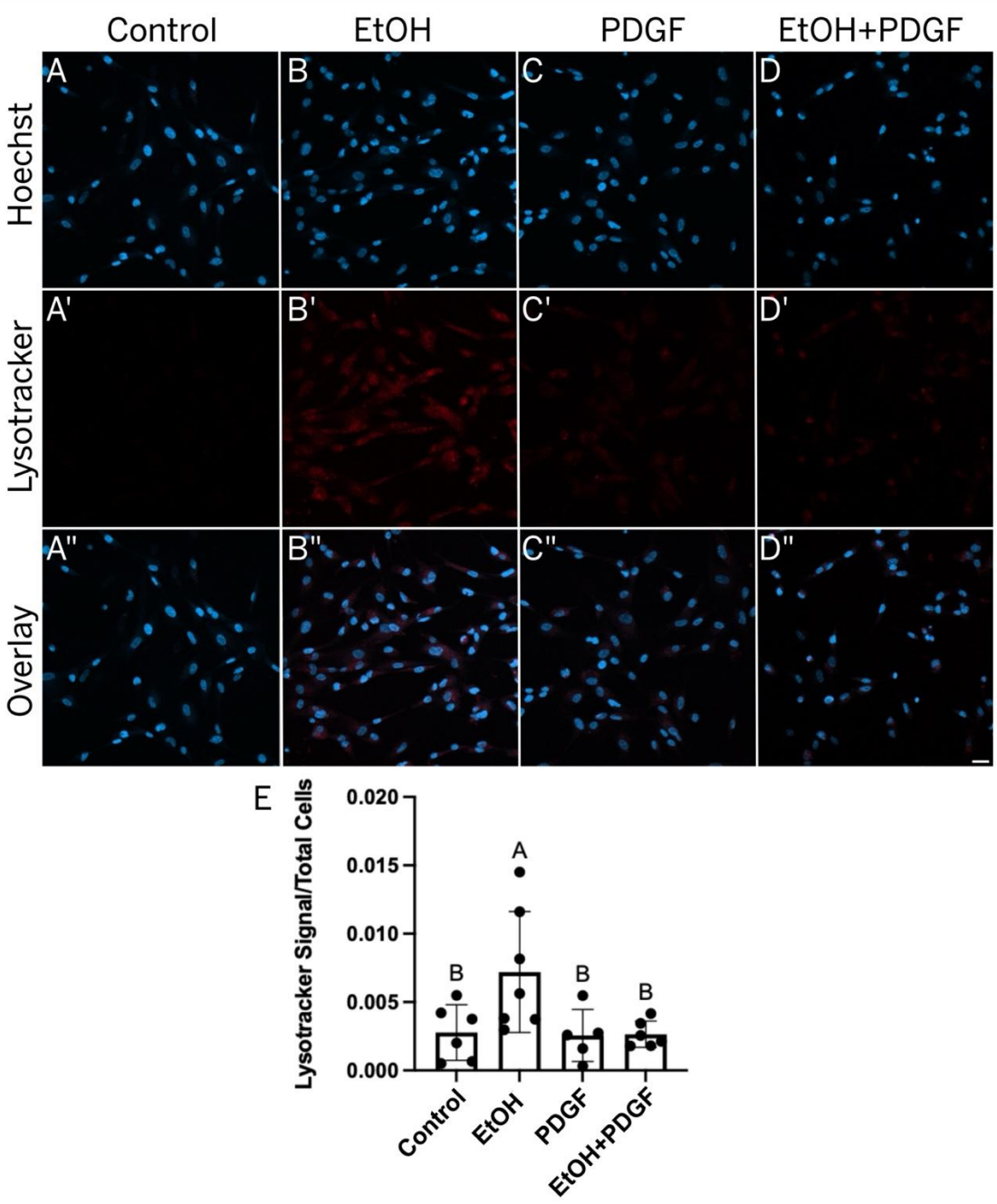


Figure 5. PDGFRA signaling protects against ethanol-induced autophagy in human neural crest-like cells. (A-D) Representative Lysotracker staining for Human neural crest-like cells after 60 min incubation. (B) Autophagy is elevated in cells exposed to ethanol relative to other groups. Scale bar: 20 μm. (E) Quantification of Lysotracker fluorescence intensity across groups (one-way ANOVA, $n \geq 5$ per group; Groups that share a letter are not statistically significant from one another; error bars represent SD). EtOH: ethanol.

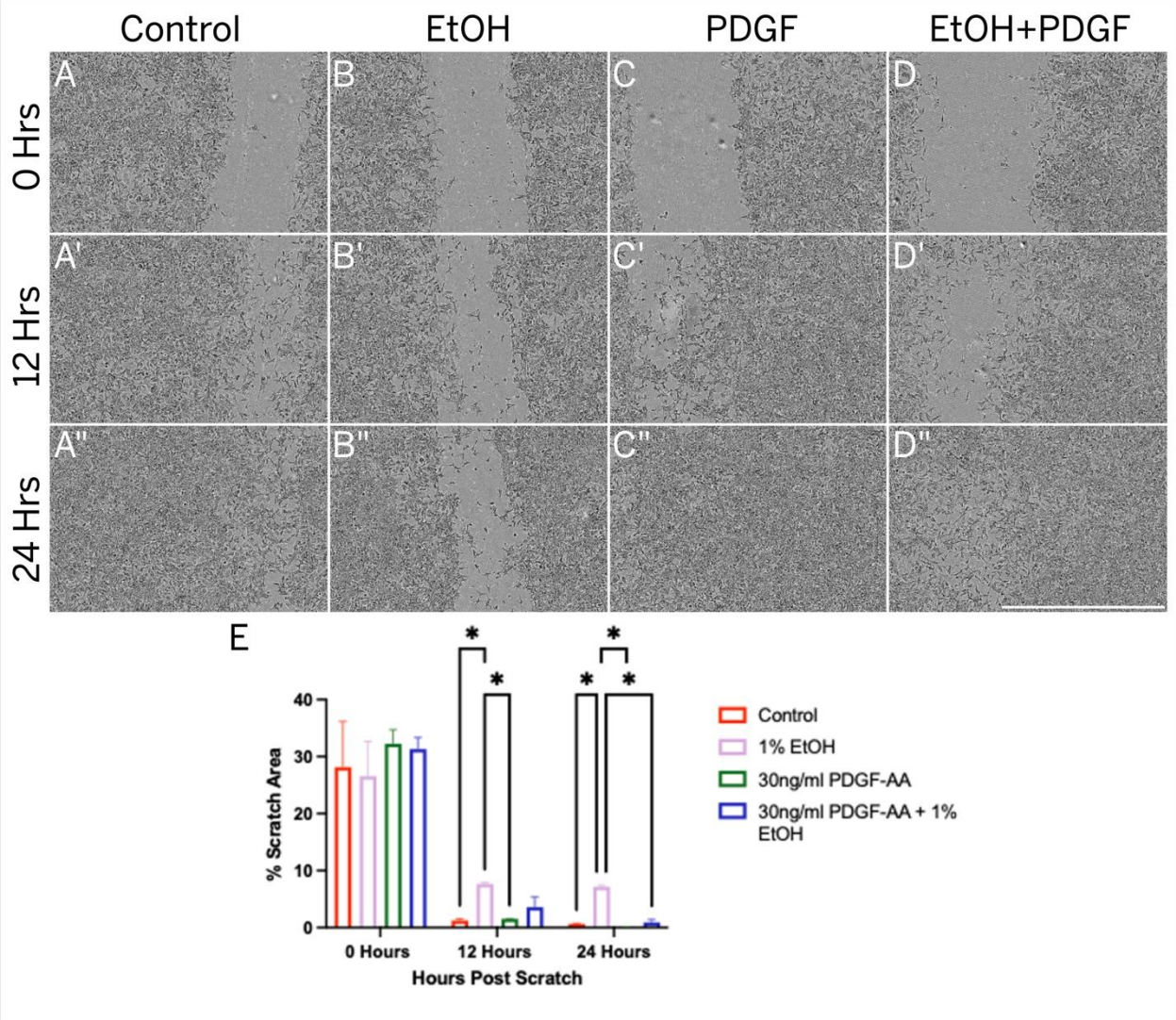


Figure 6 PDGF signaling ameliorates wound closure in ethanol-exposed cells. (A-D) Scratch assays of human neural crest-like cells treated with (B) ethanol, (C) PDGF-AA, or (D) both. (E) Quantification of precent area of scratch uncovered across treatment groups at each time point (two-way ANOVA, $n \geq 3$ per group; *$p < 0.05$; error bars represent SD). Within 12 hours control and PDGF-AA treated cells have migrated significantly more than cells exposed to ethanol, with or without PDGF-AA stimulation. At 24 hours after the scratch, cells treated with PDGF-AA and ethanol have migrated significantly farther than ethanol exposed cells. EtOH: ethanol. Scale bar: 1,000 um.

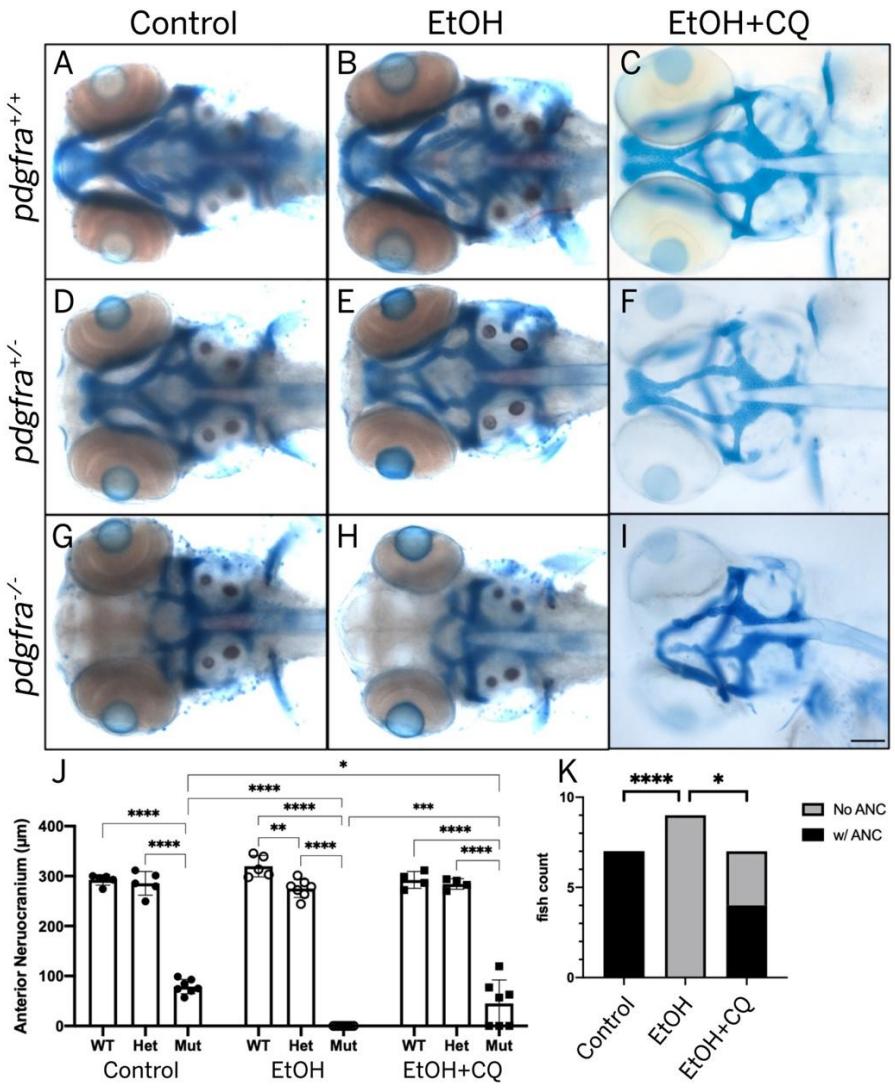


Figure 7. Inhibition of autophagy rescues craniofacial development in ethanol exposed *pdgfra* heterozygotes and mutants. (A-I) Wild-type, heterozygous, and mutant *pdgfra* embryos were treated with 1% ethanol alone or in combination with 1.5 mM chloroquine (CQ) from 6 h to 4 days post-fertilization (dpf). (J) Control heterozygotes are indistinguishable from wild-types and the anterior neurocranium is dramatically shortened in mutants. Ethanol significantly reduces the size of the anterior neurocranium in *pdgfra* heterozygotes. Chloroquine treatment fully rescues this effect. Ethanol treatment causes a complete and invariant loss of the neurocranium in *pdgfra* mutants which is partially rescued by chloroquine. (K) The proportion of *pdgfra* mutants with partial anterior neurocranium is significantly increased by chloroquine exposure, relative to ethanol alone (4/7). Scale bar: 100 µm.

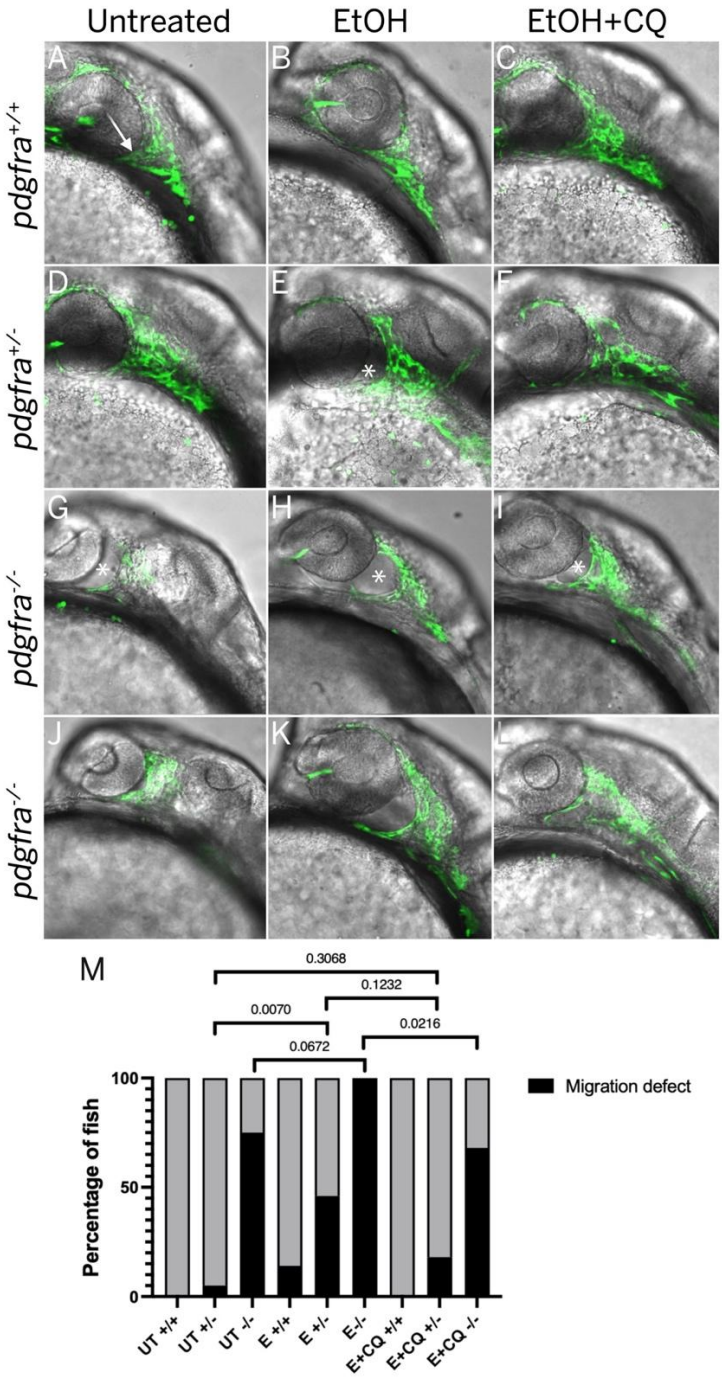


Figure 8 Inhibition of autophagy rescues neural crest cell migration in vivo. (A-L) Neural crest cell distributions in *pdgfra* wild-type, heterozygous and mutant embryos. A common defect in *pdgfra* mutants is that neural crest cells fail to properly migrate into territory adjacent to the eye (G, *). Nearly half of exposed *pdgfra* heterozygotes have a similar defect (E) and all mutants display this defect (H, K). (F, I, L) Co-treatment with chloroquine lessens these defects. (M) Quantification of migratory defects.

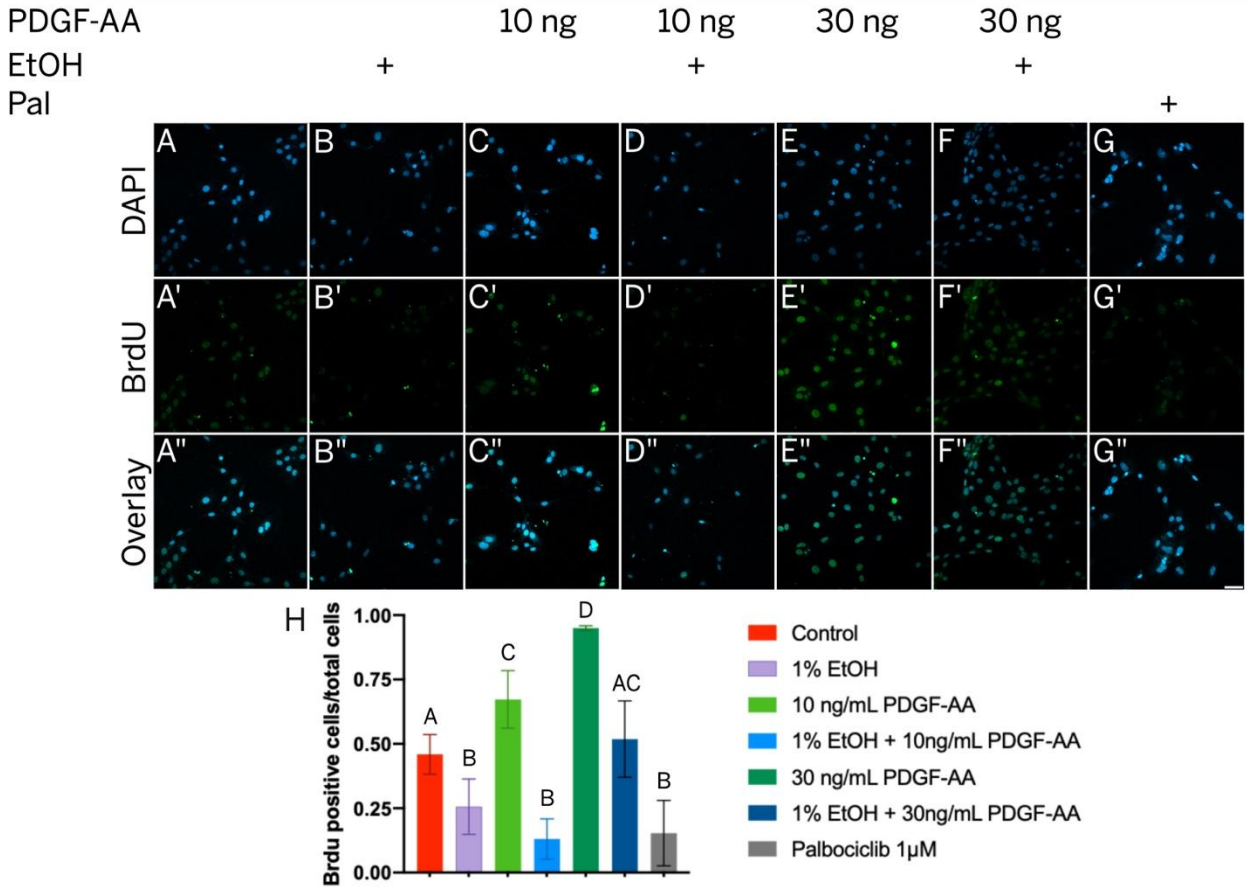


Figure S1. Ethanol reduces PDGF-AA dependent proliferation. (A, B) Ethanol exposure reduces the basal level of iMEPM cell proliferation. (C-F) Ethanol exposure reduces the PDGF-AA dose dependent increase in proliferation. (G) Treatment with Palcociclib, a proliferation inhibitor. (H) Quantification of proliferation. Groups that share a letter are not statistically significant from one another.

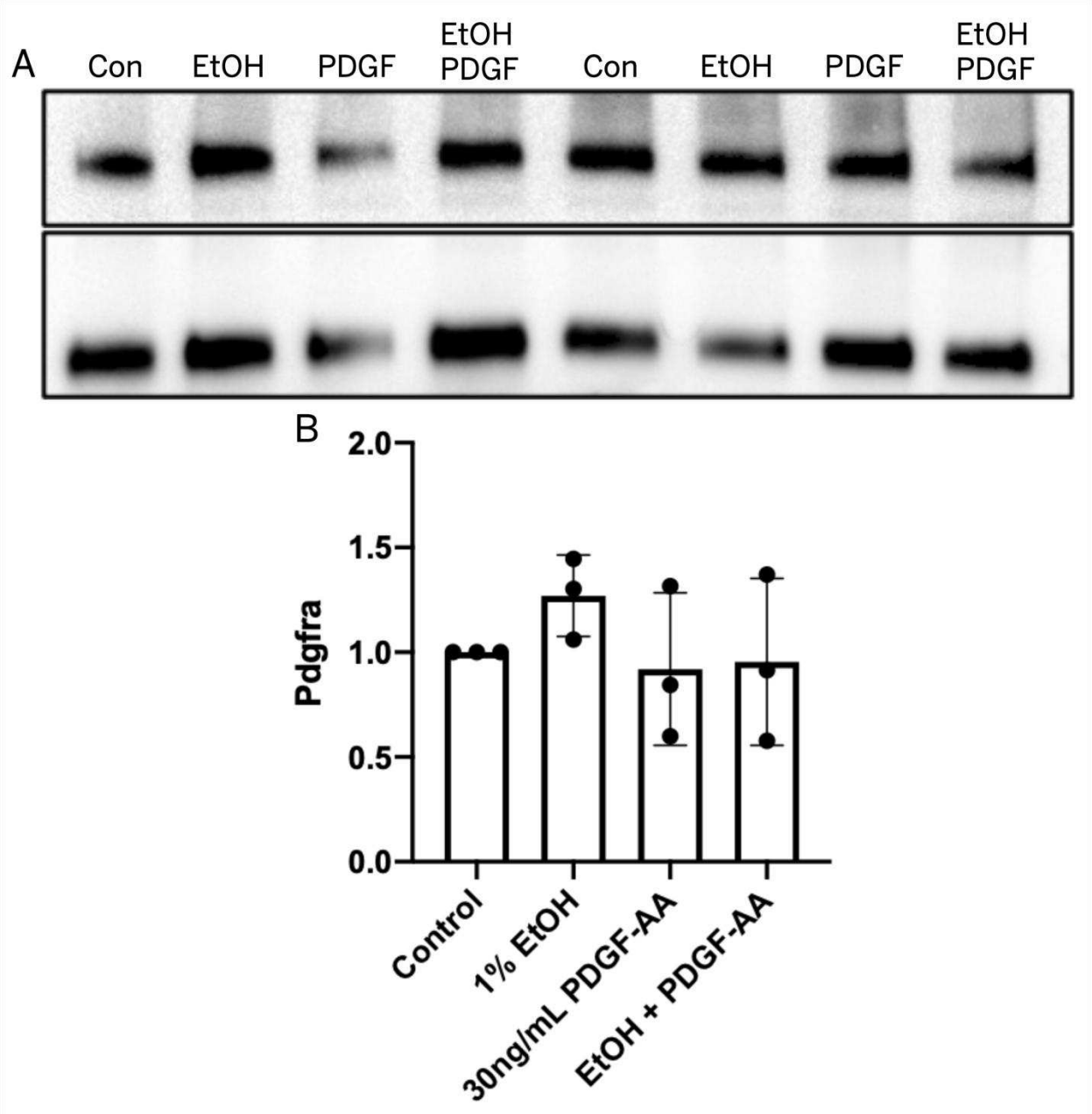


Figure S2. Ethanol does not reduce the levels of Pdgfra protein. (A) Immunoblot analysis of total levels of Pdgfra protein across treatment groups. (B) No differences in levels of the receptor were detected.

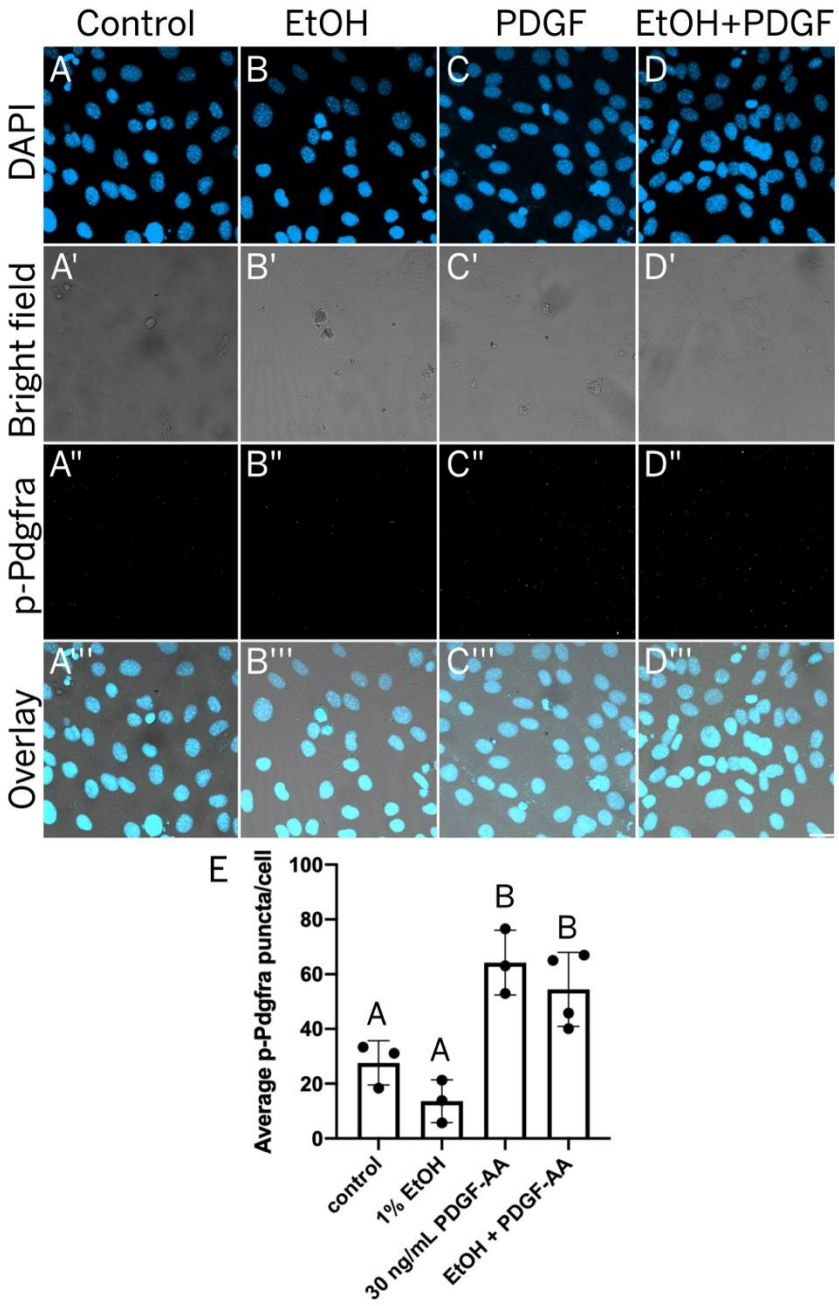


Figure S3. Phosphorylation of Pdgfra is not altered by ethanol. (A-D) iMEPM cells stainined with anti-phospho-Pdgfra antibodies. Relative to controls (A) and ethanol-exposed cells (B), cells treated with PDGF-AA (C, D) have higher levels of phospho-Pdgfra regardless of ethanol co-exposure. (E) Quantification of puncta across groups.

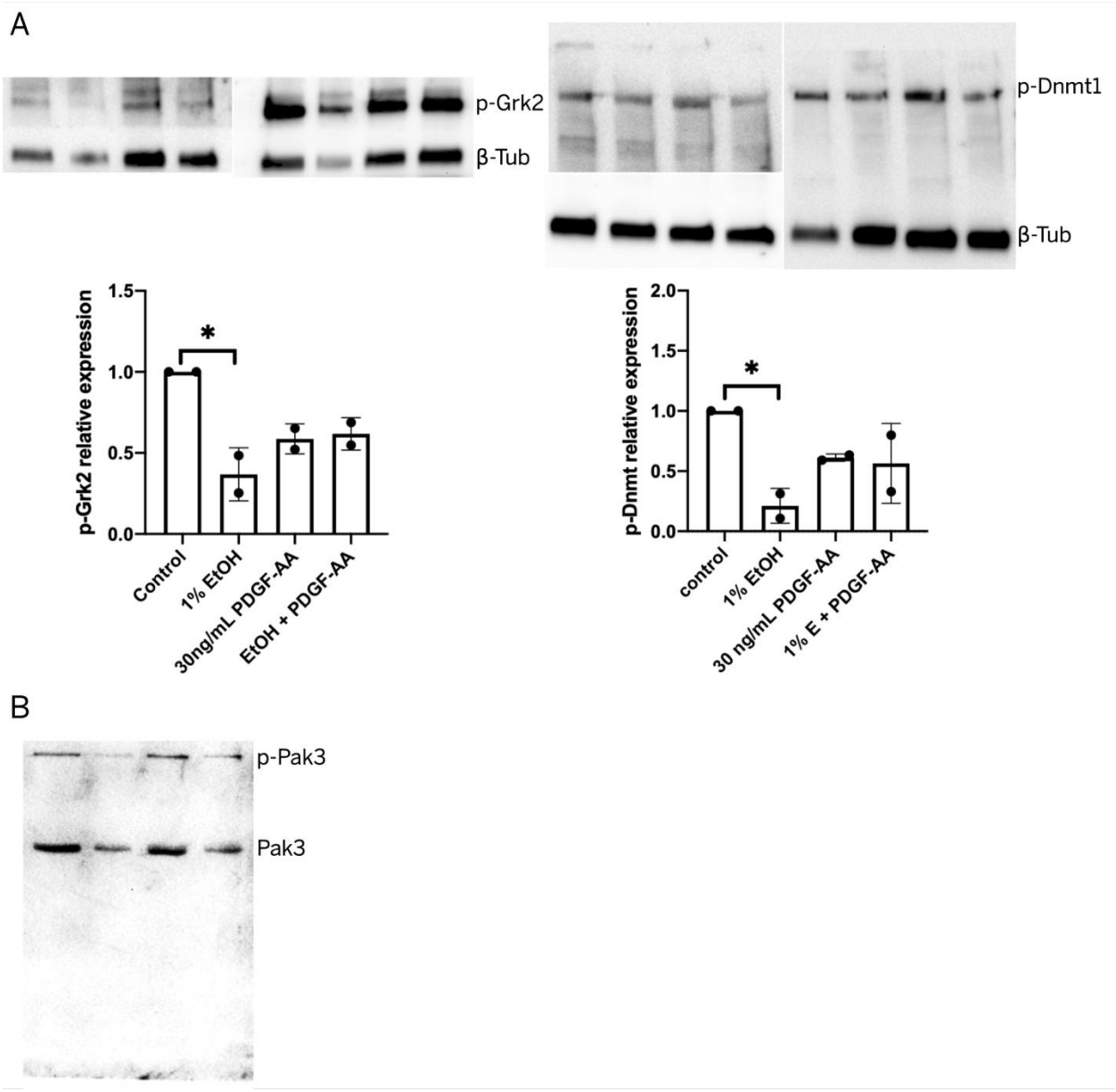


Figure S4. Phospho-proteomic validation. (A) Staining and quantification using phopho-specific antibodies to Grk2 and Dnmt1 validates the phosphoproteome data. (B) Phospho-tag staining with a Pak3 antibody.



Figure S5. Go term enrichment analysis.

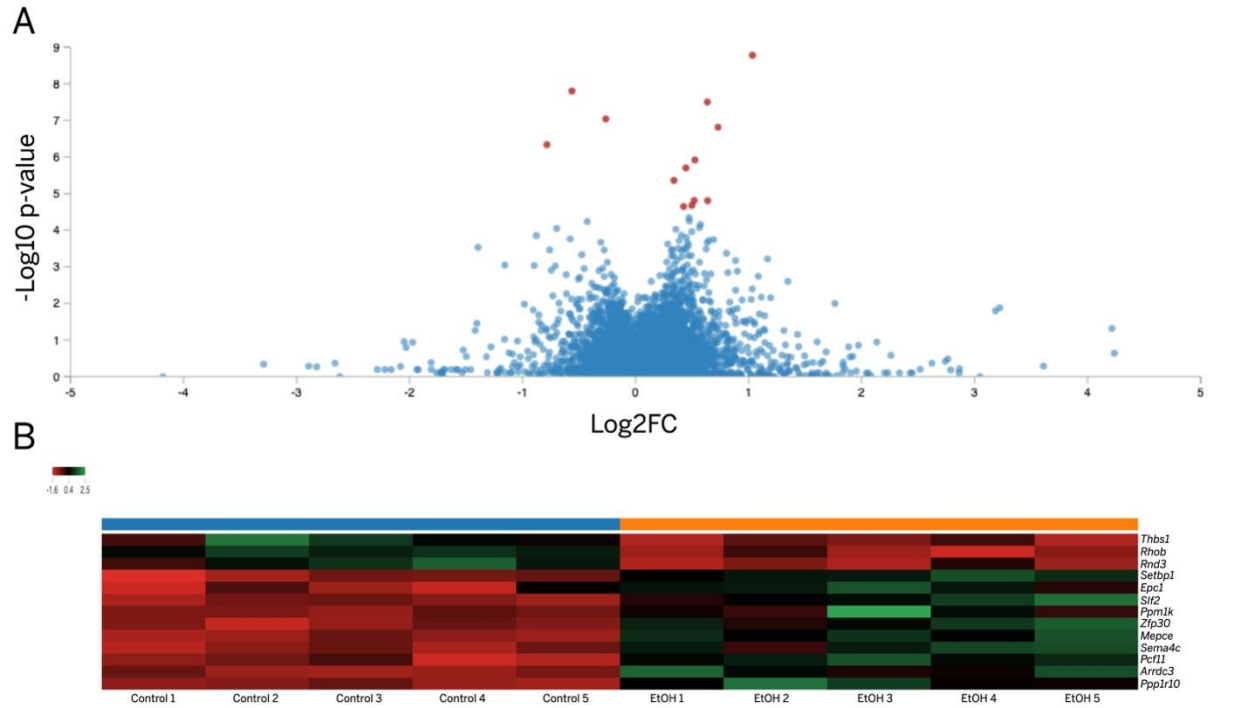


Figure S6. Transcriptomic analyses on ethanol-exposed iMEPM cells. (A) Volcano plot and (B) heatmap showing the differential expression of 13 genes in iMEPM cells treated with 1% ethanol for 1 hour.

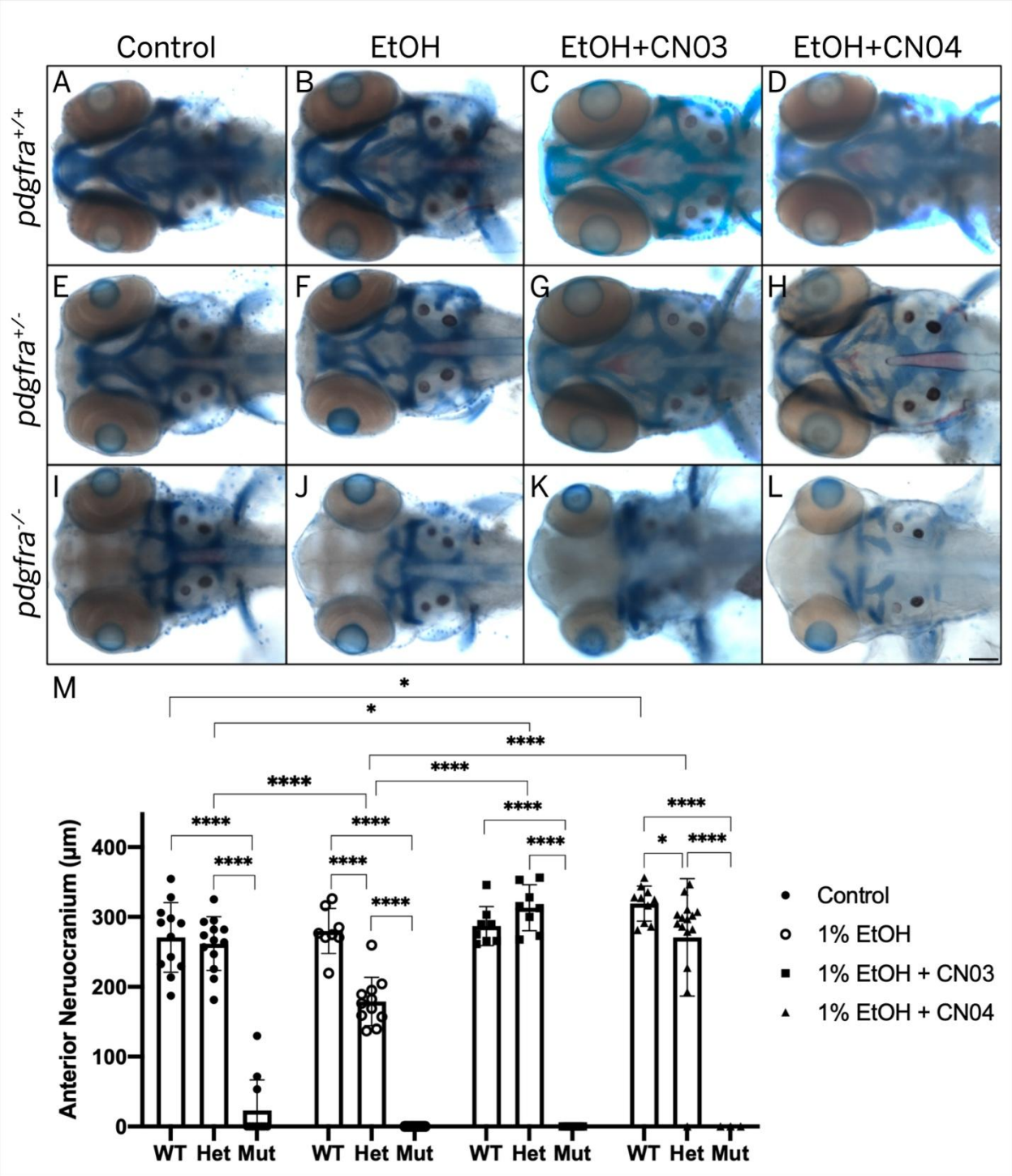


Figure S7. Activating Rho-GTPases rescues *pdgfra* heterozygotes but not mutants. (A-L) Whole mount images of zebrafish stained with Alcian Blue/Alizarin Red across *pdgfra* genotypes and treatment groups. (M) Statistical analyses demonstrate that activators of Rho-GTPase activity improve the size of the palatal skeleton in *pdgfra* heterozygotes (Het), but not homozygous mutants (Mut).

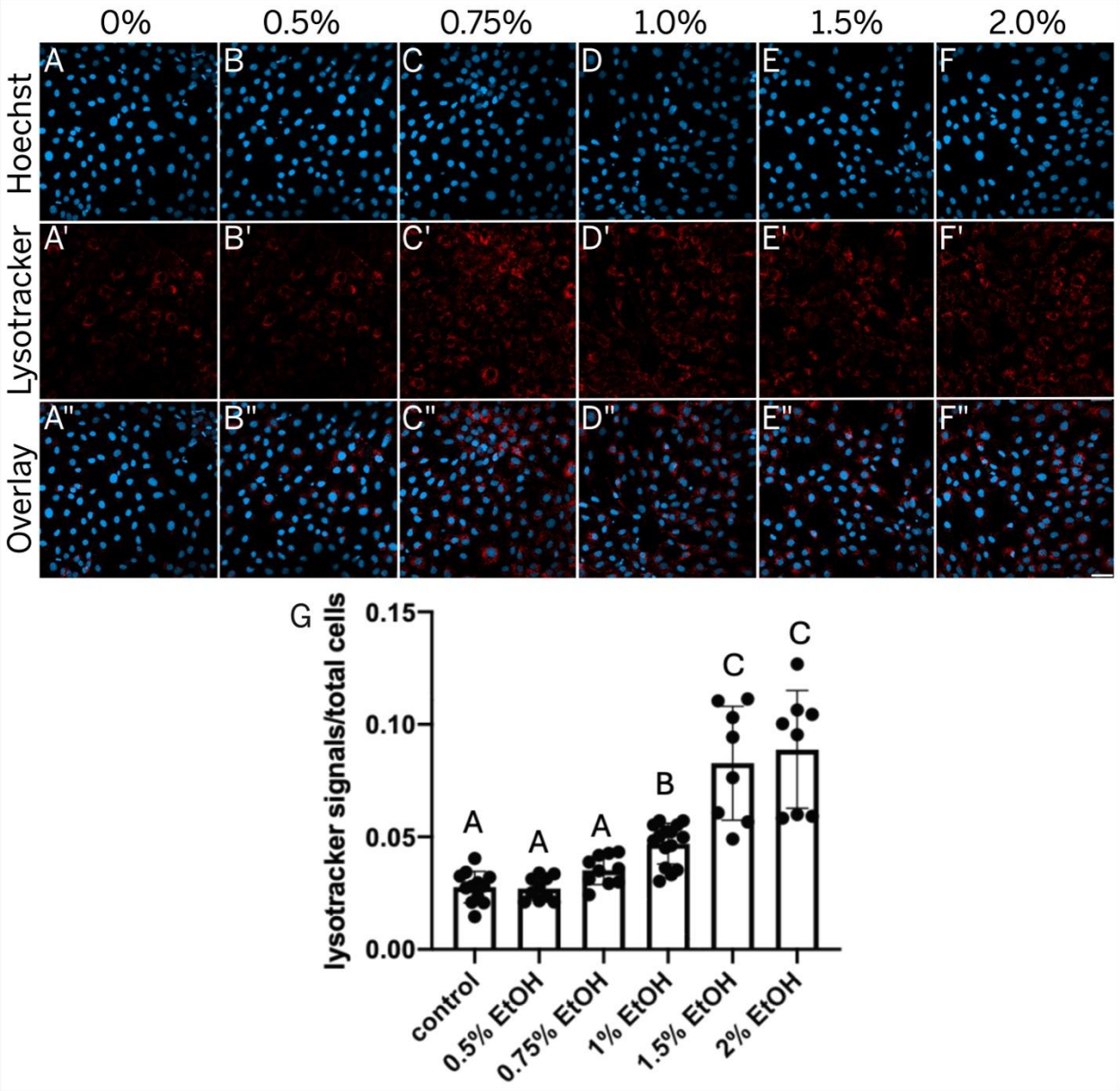


Figure S8. Autophagy is significantly elevated in cells exposed to at least 1% ethanol. (A-F) iMEPM cells stained treated with varying concentrations of ethanol and stained with Lysotracker. (G) Statistical analyses demonstrate that 1% ethanol is the lowest concentration that significantly elevates Lysotracker signal.

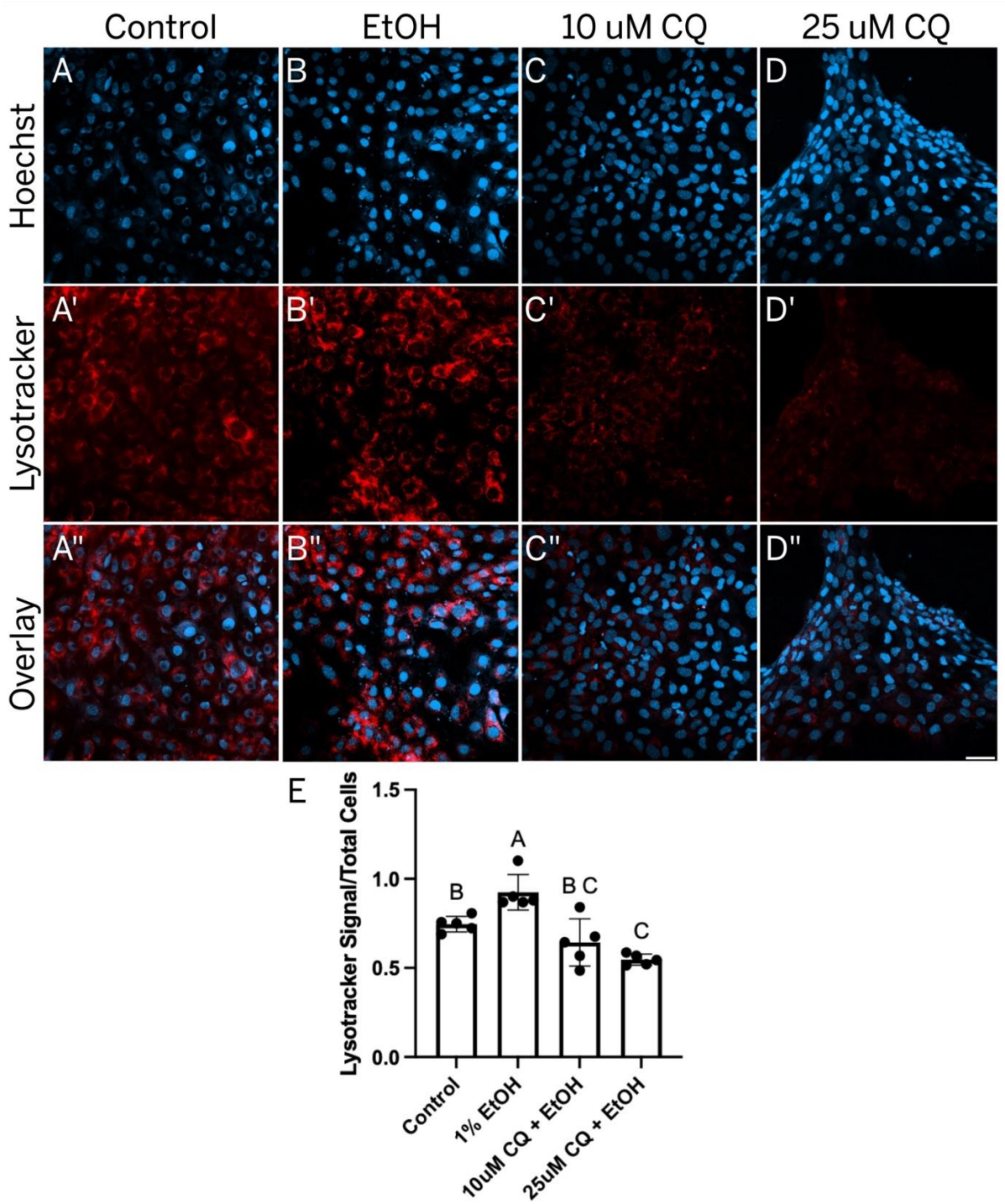


Figure S9. 10uM chloroquine reduces ethanol-induced autophagy to baseline levels. (A-D) iMEPM cells stained with LysoTracker. (A, B, E) Ethanol treatment significantly elevates signal relative to untreated cells. (C, E) Treatment with ethanol and 10 uM chloroquine restores Lysotracker signal to control, baseline, levels. (D, E). 25 uM chloroquine further reduces Lysotracker signaling in ethanol-exposed cells.

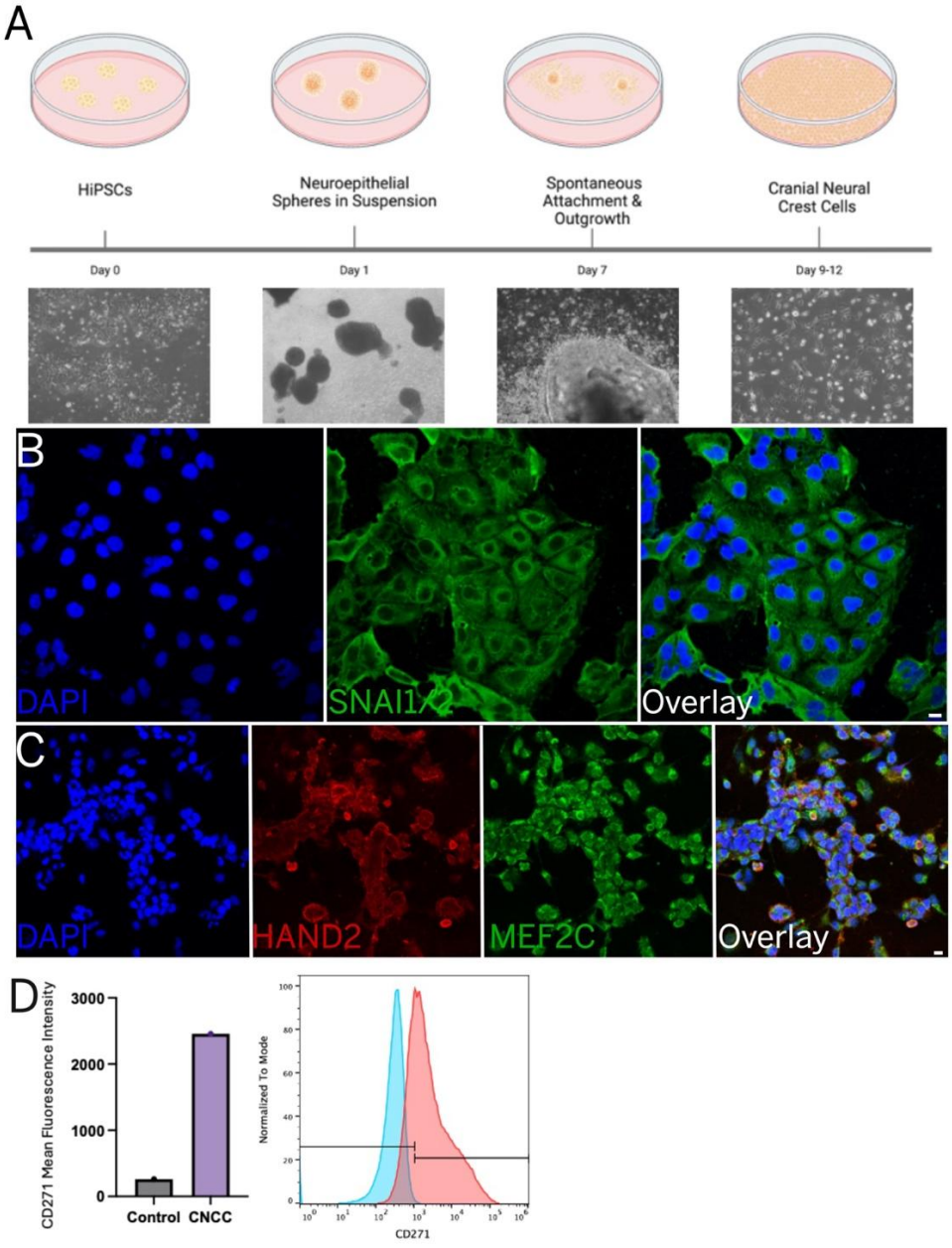


Figure S10. Differentiation of hiPSCs into cranial neural crest-like cells. (A) Differentiation protocol schematic. (B) Differentiated cells express the pan-neural crest marker SNAI1/2. (C) Differentiated cells express cranial neural crest cell markers, HAND2 and MEF2C. (D) Differentiation efficiency. The initial differentiation protocol resulted in ~90% of cells being CD271-positive. CD271-positive cells were sorted and used to establish pure neural crest-like cell cultures.

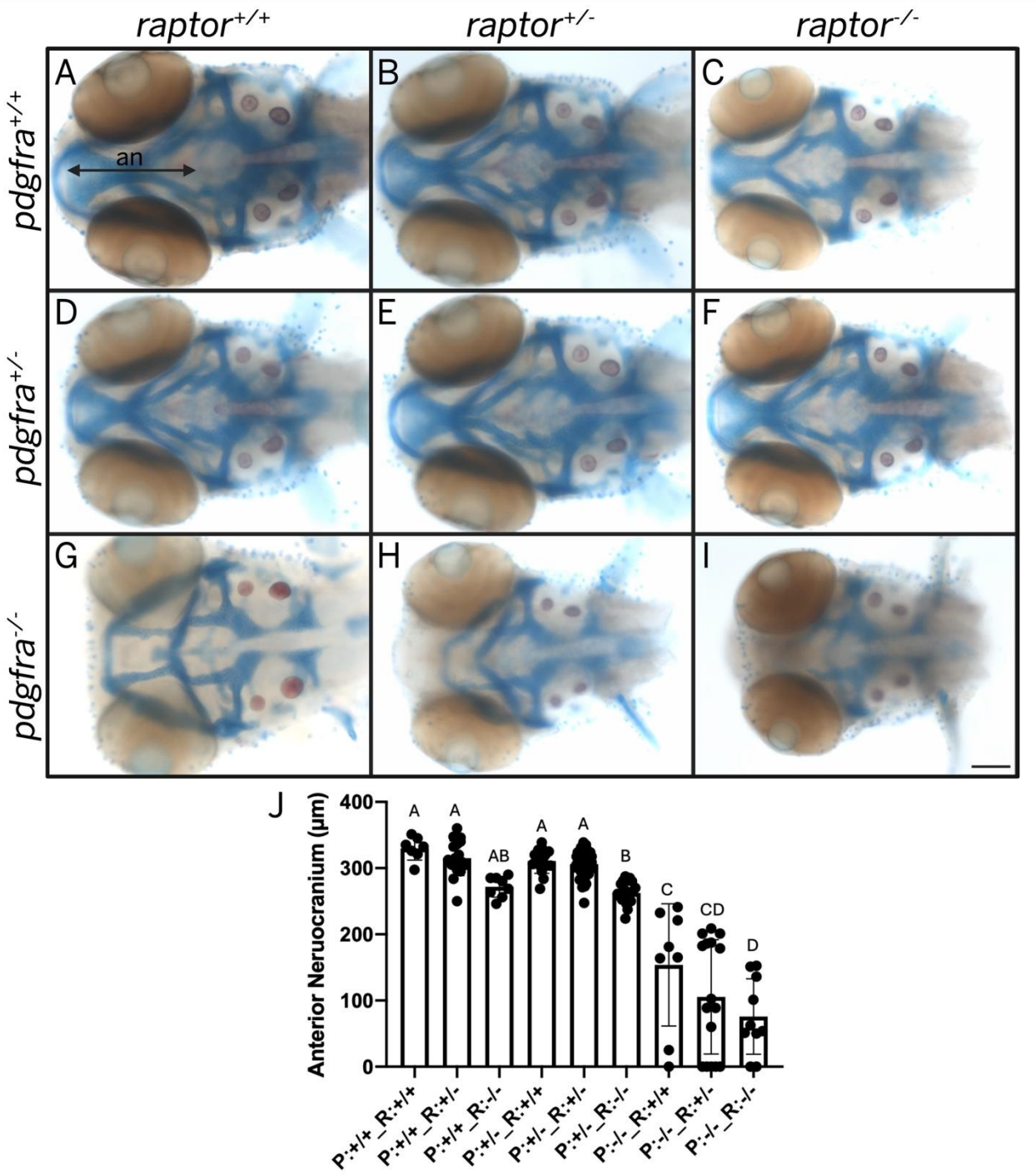


Figure S11. Genetic interaction between *raptor* and *pdgfra* during craniofacial development. (A-I) Whole mount skeletal stains of zebrafish of all allelic combinations of *pdgfra* and *raptor*. (J) Statistical analyses of neurocranial length across genotypes. Neurocrania of double mutant zebrafish are significantly reduced relative to all other genotypes.

Supplementary Files

This is a list of supplementary files associated with this preprint. Click to download.

- TableS2.xlsx
- TableS5.xlsx
- TableS3.xlsx
- TableS6.xlsx
- TableS4.xlsx
- TableS1.xlsx